AD-A055 846 NORTH CAROLINA STATE UNIV RALEIGH DEPT OF MECHANICAL--ETC F/G 20/4
DEVELOPMENT OF A COMPUTER PROGRAM TO CALCULATE AERODYNAMIC CHAR--ETC(U)
MAR 78 F R DEJARNETTE, K M JONES N60921-77-C-A066

UNCLASSIFIED NSWC/DL-TR-3829 NL

1 OF 1
ADA
055848

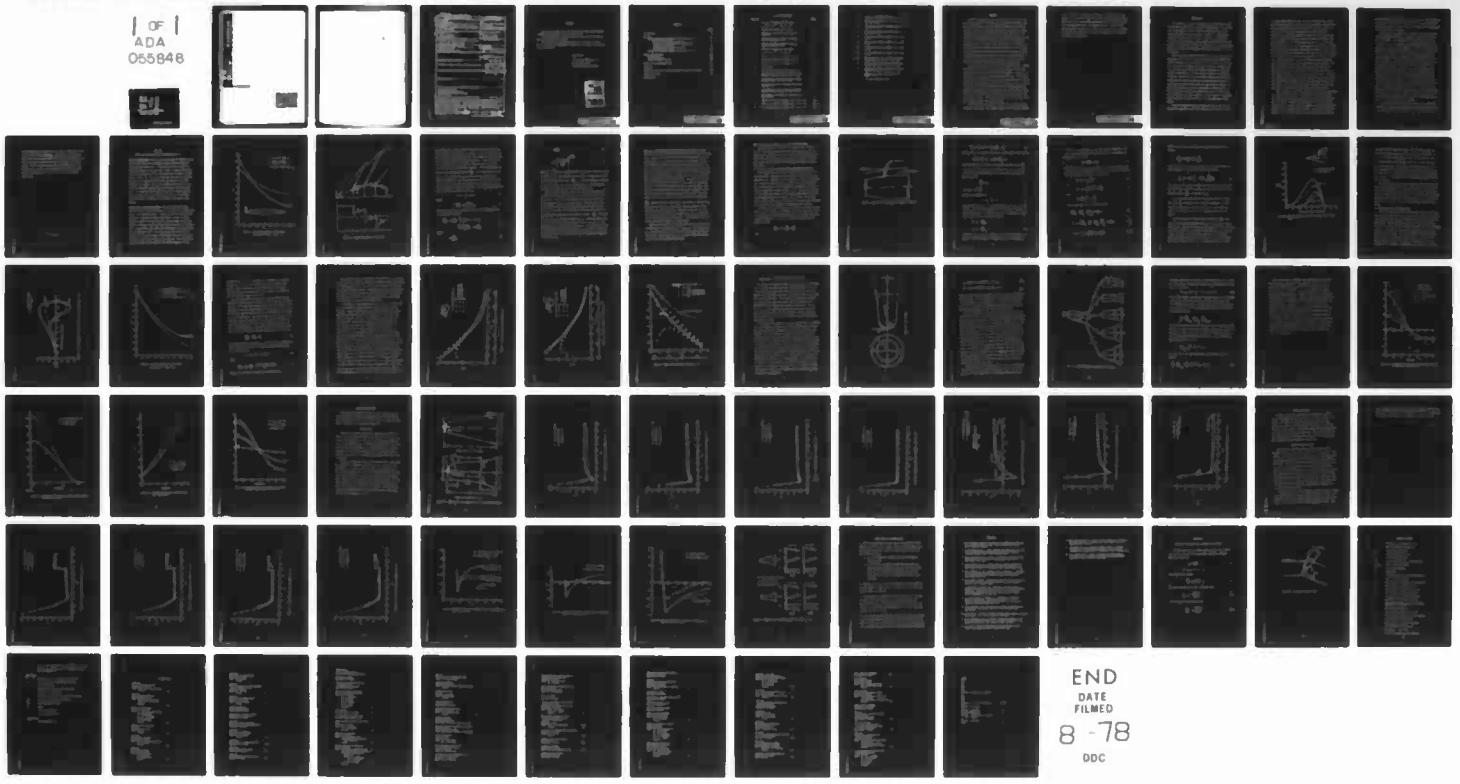

END
DATE FILMED
8-78
DDC

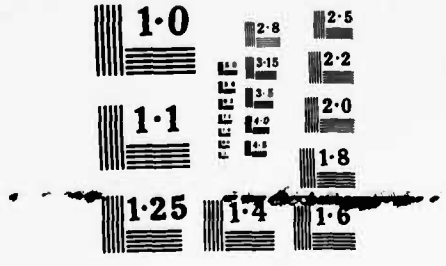

MARCH 1978

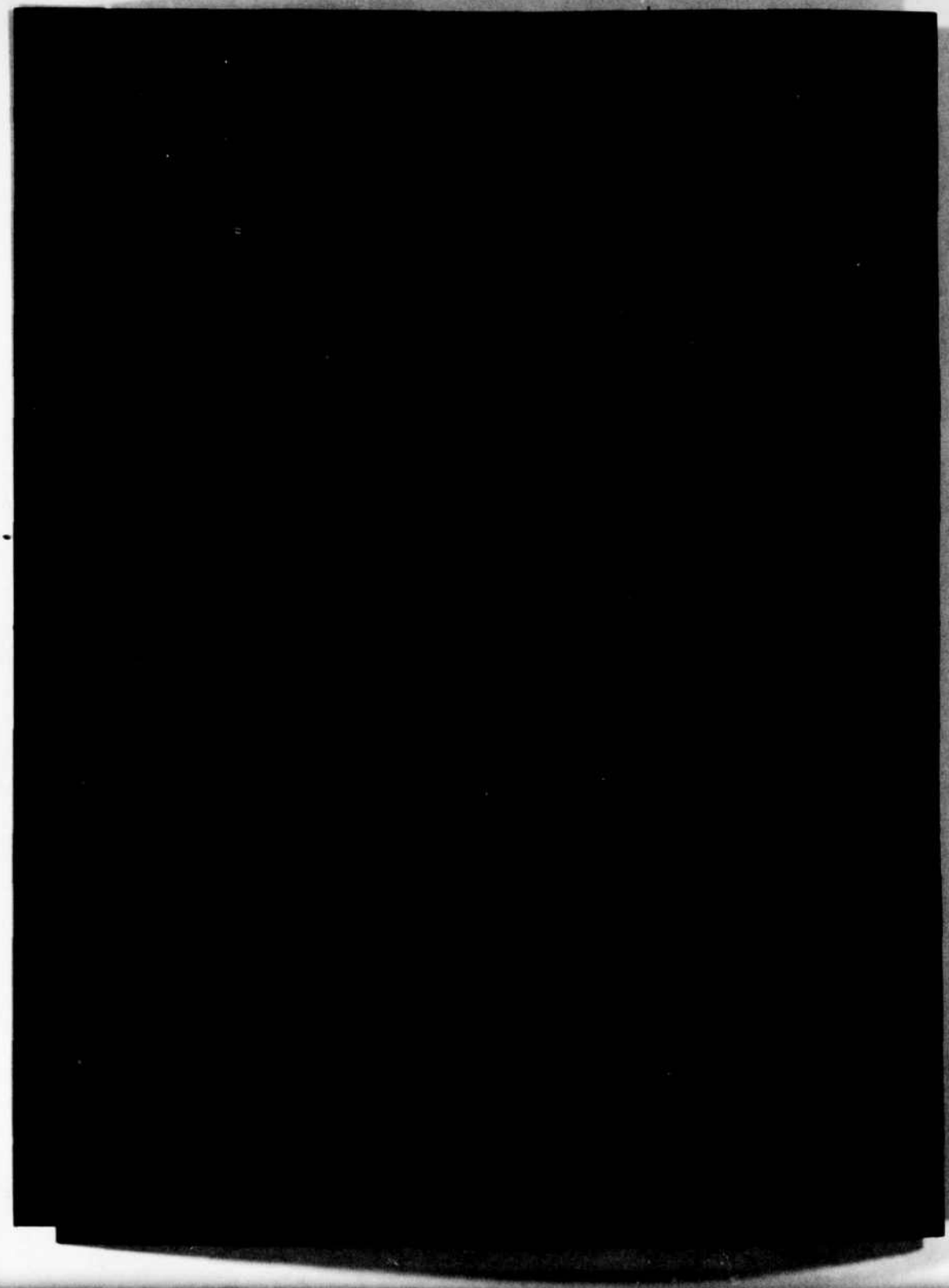

UNCLASSIFIED

SECURITY CLASSIFICATION OF THIS PAGE (When Data Entered)

REPORT DOCUMENTATION PAGE	READ INSTRUCTIONS BEFORE COMPLETING FORM
1. REPORT NUMBER: NSWC/DL TR-3829	2. GOVT ACCESSION NO. / 3. RECIPIENT'S CATALOG NUMBER
4. TITLE (and Subtitle): DEVELOPMENT OF A COMPUTER PROGRAM TO CALCULATE AERODYNAMIC CHARACTERISTICS OF BODIES AND WING-BODY COMBINATIONS.	5. TYPE OF REPORT & PERIOD COVERED: Interim Report 15 Dec 76 - 15 Dec 77 / 6. PERFORMING ORG. REPORT NUMBER
7. AUTHOR(s): Fred R. DeJarnette, Kenneth M. Jones	8. CONTRACT OR GRANT NUMBER(s): N60921-77-C-A066
9. PERFORMING ORGANIZATION NAME AND ADDRESS: Mechanical and Aerospace Engineering Department, North Carolina State University, Raleigh, North Carolina 27650	10. PROGRAM ELEMENT, PROJECT, TASK AREA & WORK UNIT NUMBERS
11. CONTROLLING OFFICE NAME AND ADDRESS: Naval Surface Weapons Center (Code K-21), Dahlgren Laboratory, Dahlgren, Virginia 22448	12. REPORT DATE: March 1978 / 13. NUMBER OF PAGES: 81 (12) 69p.
14. MONITORING AGENCY NAME & ADDRESS (if different from Controlling Office)	15. SECURITY CLASS. (of this report): Unclassified / 15a. DECLASSIFICATION/DOWNGRADING SCHEDULE

16. DISTRIBUTION STATEMENT (of this Report)

Approved for public release; distribution unlimited

DDC RECEIVED JUN 28 1978 B

17. DISTRIBUTION STATEMENT (of the abstract entered in Block 20, if different from Report)

18. SUPPLEMENTARY NOTES

19. KEY WORDS (Continue on reverse side if necessary and identify by block number)

Supersonic Mach Number
Surface Pressure Distribution
Second-Order Shock-Expansion Method
Angle of Attack

20. ABSTRACT (Continue on reverse side if necessary and identify by block number)

A new method has been developed for calculating an approximate surface pressure distribution over axisymmetric bodies, with pointed or blunted noses, at angle of attack in supersonic flow. A modified form of the second-order shock-expansion method is developed and matched to modified Newtonian theory near the nose. Surface pressure distributions compared well with experimental data on blunted cones with and without flares at Mach numbers from 1.5 to 4.63 and angles of attack to 12°.

78 06 16 013

DD FORM 1 JAN 73 1473 EDITION OF 1 NOV 65 IS OBSOLETE

UNCLASSIFIED

SECURITY CLASSIFICATION OF THIS PAGE (When Data Entered)

400 714

FOREWORD

This technical report covers the work performed under Contract N60921-77-C-A066 from 15 December 1976 to 15 December 1977.

The funding support for this work was provided by the Office of Naval Research Task Number RF 32-391-801.

This report was reviewed and approved by Dr. J. Sun; Dr. L. Devan; Dr. F. G. Moore, Head, Aeromechanics Branch; and H. P. Caster, Head, Exterior Ballistics Division.

Released by:

R. A. NIEMANN, Head
Strategic Systems Department

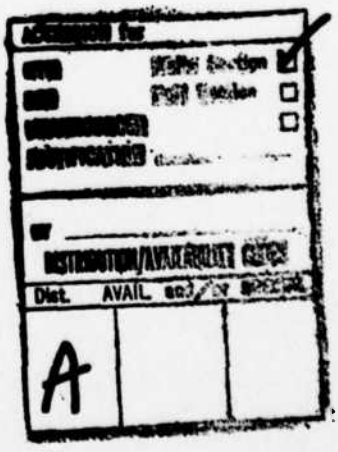

CONTENTS

LIST OF ILLUSTRATIONS

SUMMARY

The optimal aerodynamic design of new configurations requires computer programs which will calculate surface pressure distributions efficiently and reasonably accurately. Numerical methods which calculate the entire inviscid flow field require computational times and storage too large to use in design optimization processes. Therefore, a new method has been developed for calculating an approximate surface pressure distribution over axisymmetric bodies, with pointed or blunted noses, at angle of attack in supersonic flow. This method is an extension and modification to the second-order shock-expansion method which was originally developed for pointed bodies near zero angle of attack. The modified Newtonian pressure distribution is used in the nose region back to a "matching" point where the local Mach number is slightly supersonic. Then the new method is applied downstream of the matching point.

In the late 60's Jackson, et al, of NASA Langley determined a different matching point, but it did not pick up the overexpansion near the juncture at sphere-cones at low supersonic Mach numbers. The use of the new matching point predicts this overexpansion quite well. One modification made to the basic second-order shock-expansion method was the development of an "exact" method for calculating the pressure gradient at corners to replace the approximate method normally used. Another modification made was the development of a new method to calculate the effective cone pressure to replace the tangent cone pressure typically used for bodies at an angle of attack. This effective cone pressure was found to be much more accurate than the tangent cone pressure.

The new method has been applied to sphere-cones and sphere-tangent ogive-cone-flare bodies. Mach numbers ranged from 1.5 to 4.63 and angles

of attack up to 12°. Surface pressure distributions were found to compare well with experimental data. In addition, the resulting axial force, normal force, and pitching moment coefficients were also found to compare well with experimental data. The computer program is relatively fast, requiring about 15 seconds for a typical case on the IBM 370/165 computer. The accuracy and simplicity of this computer program makes it attractive for engineering applications.

INTRODUCTION

Present and future mission requirements of the Navy dictate a need for methods to design optimum aerodynamic configurations. Of particular interest are methods which will predict the static and dynamic aerodynamic characteristics of wings, bodies, and wing-body combinations throughout the speed regimes of subsonic, transonic, and supersonic flow and at angles of attack. Since a number of configurations must be analyzed in an optimization process, it is imperative that the techniques employed to calculate the aerodynamic coefficients be efficient as well as accurate.

There are generally three approaches which could be used to estimate aerodynamic coefficients. First, wind tunnel and ballistic range tests could be employed, but they are expensive, time-consuming, and additional tests are required for new configurational innovations. Secondly, hand calculations can be performed using handbook techniques, but they also require a large number of man hours and their accuracy is questionable or unknown. The third method is to develop a computer program based on a combination of analytical techniques and semi-empirical methods. Although the third method is also costly and time-consuming initially, it allows the designer to calculate a large number of configurations and flight conditions accurately and expeditiously, and it is ideal for design optimization techniques. Therefore, the third method is considered the best approach for long-term use and it is the method used in this report.

A number of computer programs have been developed to calculate the aerodynamic characteristics of flight vehicles, but none of them covers

the range of Mach numbers ($0 < M_\infty < 6$), angles of attack ($0 \leq \alpha \leq 15°$), and complete configurations which are of present concern. Quite general body and wing geometries are of current interest, and they include spin stabilized bodies and guided and unguided fin stabilized bodies. Woodward[1] used a perturbation method to compute the pressure distribution on wing-body combinations at subsonic and supersonic speeds. However, his method does not include blunted bodies, transonic flow, skin friction drag, base drag, and nonlinear angle of attack effects. Jackson and Smith[2] used the second-order shock-expansion theory[3] to calculate the drag on pointed bodies of revolution at zero angle of attack in supersonic flow. They also calculated the pressure and skin-friction drag but did not include the base drag. Jackson, et al[4] modified the second-order shock expansion method for blunt-nosed bodies and angle of attack. This method was found to predict the pressure distribution and force and moment coefficients on blunted cones and blunted-cones with flares at Mach numbers from about 1.5 to 5 and angles of attack to 12°. Of particular importance was the fact that their adaptation of the second-order shock expansion method predicted some of the over expansion near the sphere-cone juncture at Mach numbers greater than about 2.0. However, below Mach 2 the pressure prediction near the shoulder was poor.

Another method for calculating aerodynamics of wing-body combinations is that due to Saffell et al[5]. It is only applicable to low aspect-ratio configurations, and the drag calculations are inaccurate at small angles of attack. An empirical method called the "Spinner" program[6] was developed by the General Electric Company for spin-stabilized bodies, however it will not handle guided vehicles. There are several computer programs, e.g., Solomon et al[7], which use finite-difference methods to

calculate the entire flow field around a body. However, these techniques are generally limited to inviscid supersonic flow over bodies without wings or fins, and they require computational times much too large to use in design optimization processes.

The best computer program which is currently available to compute static aerodynamic characteristics of general wing-body geometries is the one by Moore[8]. This program predicts the pressure distribution, lift, drag, and center of pressure for Mach numbers from zero to three and angles of attack to fifteen degrees. The results compare well with experimental data and other analytical results. Also, a typical computation costs only about five dollars per Mach number to compute the static aerodynamic characteristics of wing-body configurations on the CDC 6700 computer. For the pressure distribution over the body alone, Moore employed Van Dyke's second-order perturbation method[9]. Since this method is designed for pointed bodies, Moore used the modified Newtonian pressure distribution near the nose of blunted bodies and then matched it with Van Dyke's second order perturbation method for the region downstream of the nose. This procedure was shown to yield surface pressures which compared well with experimental data on blunted cones at Mach numbers less than about 2.5 or 3.0. In particular, it picked up the over-expansion of the pressure near the shoulder, whereas the second-order shock-expansion method was found to be more accurate at Mach numbers greater than about 2.5 to 3.0. At these Mach numbers there is no over-expansion near the shoulder.

A two-year contract was initiated in December 1976 at the North Carolina State University to extend Moore's method to Mach numbers from 2.5 to 6 at angles of attack from zero to 15°. This report describes

the work completed during the first year of this contract which is restricted to body-alone aerodynamics. Modifications are made to the second-order shock-expansion method to calculate the pressure distributions over blunted or pointed nose bodies with flared or boattailed bodies. The skin-friction and base drag are computed from the same techniques used by Moore. The resulting pressure distribution, skin friction, and base drag are integrated to yield force and moment coefficients.

ANALYSIS

Method for Predicting Pressure Distribution at $\alpha = 0$

Modified Maslen Method - The first method considered for calculating the pressure distribution over axisymmetric bodies was Maslen's method[10]. This method was modified for $\alpha = 0$ and used by the first author[11] for blunt-nosed bodies in hypersonic flows. Figure 1 compares the pressure distribution computed by Maslen's method with that of Solomon's method[7] for $M_\infty = 3$ and $\alpha = 0$. This figure illustrates the inability of Maslen's method to pick up the over-expansion near the shoulder at the lower supersonic Mach numbers. At hypersonic speeds the over-expansion does not occur and Maslen's method predicts the pressure distribution very well. It is apparent that the approximations used in Maslen's method are not accurate at the lower supersonic Mach numbers, and therefore this technique was discarded for the applications considered in this project.

Second-Order Shock-Expansion Method - The basic second-order shock-expansion method was developed by Syvertson and Dennis[3] for pointed bodies near $\alpha = 0$ at supersonic speeds. In order to apply this method, the actual body is replaced by a tangent body which is a series of conical frustrums tangent to the actual body at a selected number of positions. Figure 2 illustrates a typical pointed body and the corresponding tangent body. The pressure on the initial cone is obtained from a cone solution, e.g., the method of Sims[12]. The pressure along that initial cone is constant, but the pressure drops discontinuously across the juncture of the initial cone and the following conical frustrum. This pressure drop can be calculated from the standard Prandtl-Meyer expansion. In the

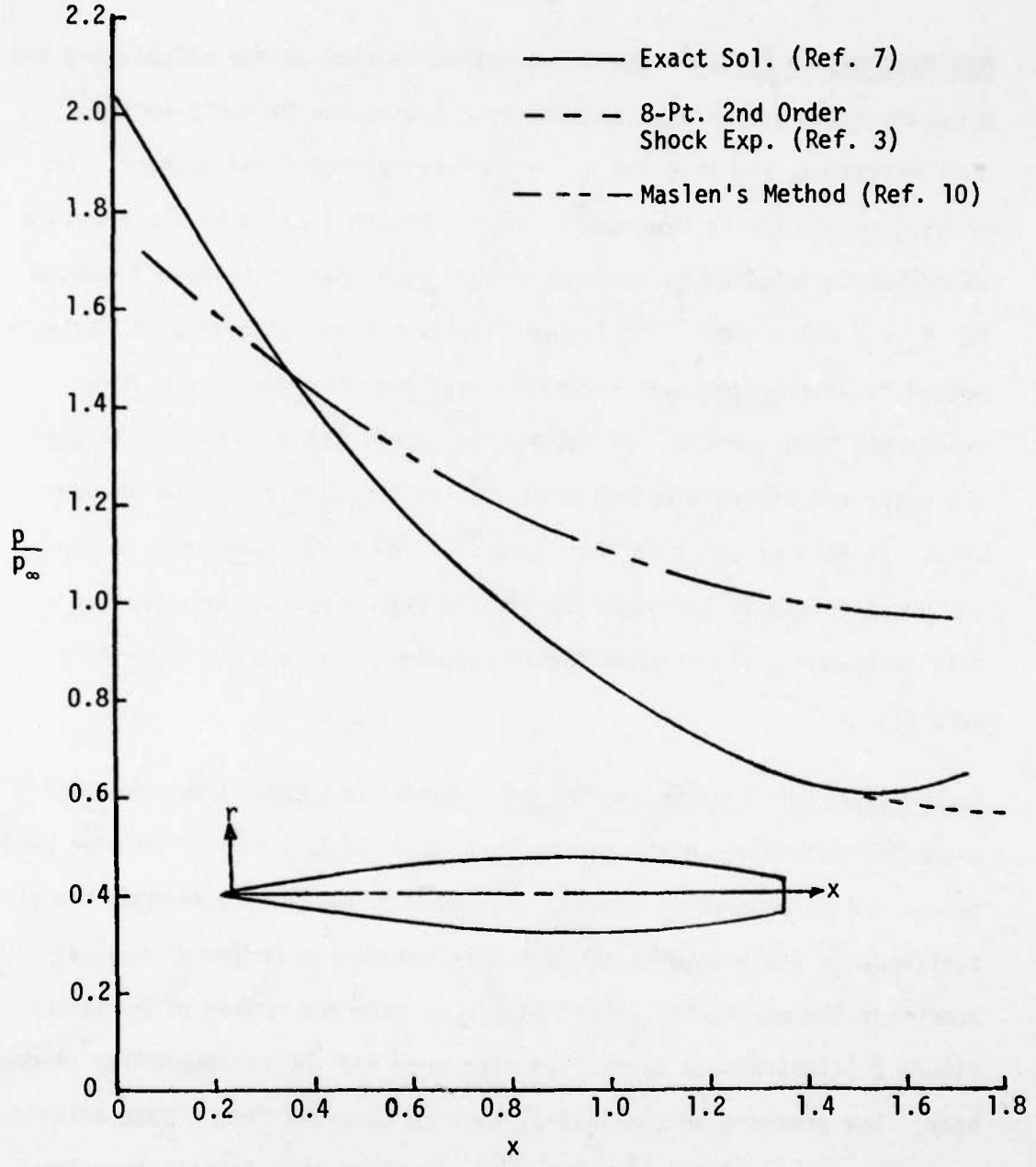

Figure 1. Pressure Distribution on Body Shape
$r=(15+2x-x^2)^{1/2}-\sqrt{15}$, $M_\infty=3$

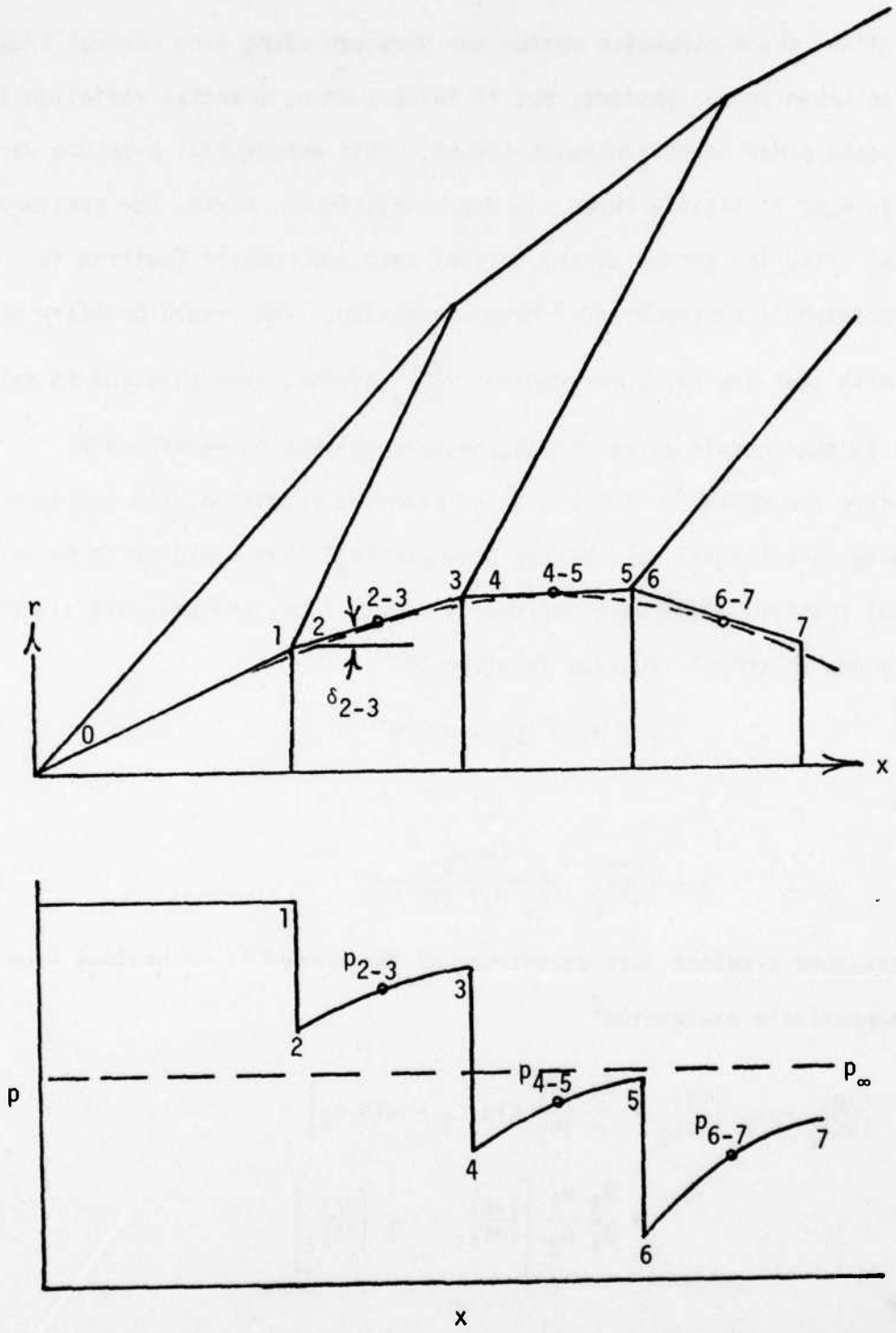

Figure 2. Tangent Body Geometry and Pressure

generalized shock-expansion method the pressure along each conical frustrum is taken to be constant, but it follows an exponential variation in the second-order shock-expansion method. This exponential pressure variation is made to satisfy three boundary conditions. First, the pressure p_2 just after the corner of the initial cone and conical frustrum is that obtained from the Prandtl-Meyer expansion. The second boundary condition is that the pressure gradient $\left(\frac{\partial p}{\partial s}\right)_2$ at this same position is set equal to that obtained from an approximate expression developed by Syvertson and Dennis[3]. For the third boundary condition, the pressure at infinity is set equal to the cone pressure (p_c) that would exist on this conical frustrum if it were infinitely long. Thus, the pressure distribution along a conical frustrum is given by

$$p \approx p_c - (p_c - p_2)\, e^{-\eta} \tag{1}$$

where

$$\eta = \left(\frac{\partial p}{\partial s}\right)_2 \frac{(x-x_2)}{(p_c-p_2)\cos \delta_2} \tag{2}$$

The pressure gradient just downstream of the corner is determined from the approximate expression[3]

$$\left(\frac{\partial p}{\partial s}\right)_2 - \lambda_2 \left(\frac{\partial \delta}{\partial s}\right)_2 = \frac{B_2}{r}\left(\frac{\Omega_1}{\Omega_2} \sin \delta_1 - \sin \delta_2\right) + \frac{B_2}{B_1}\frac{\Omega_1}{\Omega_2}\left[\left(\frac{\partial p}{\partial s}\right)_1 - \lambda_1 \left(\frac{\partial \delta}{\partial s}\right)_1\right] \tag{3}$$

where

$$B = \frac{\gamma p M^2}{2(M^2-1)} \tag{4}$$

$$\lambda = \frac{2\gamma p}{\sin 2\mu} \tag{5}$$

$$\Omega = \frac{1}{M}\left[\frac{1 + \frac{(\gamma-1)}{2} M^2}{\left(\frac{\gamma+1}{2}\right)}\right]^{\frac{(\gamma+1)}{2(\gamma-1)}} \tag{6}$$

Note that $\left(-\frac{\partial\delta}{\partial s}\right)$ is the curvature of the surface which is zero on conical frustrums, and Ω is the one-dimensional area ratio. For the first conical frustrum after the initial cone, $\left(\frac{\partial p}{\partial s}\right)_1 = 0$ since the pressure is constant on the initial cone. The pressure gradient ahead of subsequent conical frustrums is obtained from the derivative of Equation (1).

As illustrated in Figure 2, the pressure obtained from Equation (1) is used only at the position where the conical frustrum is tangent to the actual body. If the conical frustrum has a negative cone angle, Reference 3 suggests using $p_c = p_\infty$ on that segment. Reference 3 also gives an expression for the pressure gradient downstream of a sharp concave corner such as a flare. One restriction on the method described here is that the pressure gradient just downstream of a corner, $\left(\frac{\partial p}{\partial s}\right)_2$ must have the same sign as the pressure difference $(p_c - p_2)$. Otherwise, Equation (1) will not yield the third boundary condition that $p = p_c$ as $x \to \infty$. For more details of this technique, see Reference 3. In the generalized shock-expansion method, the pressure along each conical frustrum is taken to be constant and equal to the value obtained from the Prandtl-Meyer expansion at the corner, p_2.

Jackson, et al[4] Modifications to Second-Order Shock-Expansion Method

The original second-order shock-expansion method was developed for pointed noses. Jackson, et al[4] modified it for blunt nosed bodies by using the modified Newtonian pressure distribution up to a "matching-point" and then applying the second-order shock-expansion method downstream of that point. They found that the best matching point corresponded to the point on the blunted nose where the body slope is the same as the maximum wedge angle for an attached shockwave. A tangent body is used to replace the actual body downstream of the matching point. The pressure on the first conical frustrum tangent to the matching point is taken to be constant and equal to the modified Newtonian pressure for that body angle. The pressure distribution downstream of the first conical frustrum is calculated by the original second-order shock-expansion method[3]. For those conical frustrums which have the sign of the initial pressure gradient $\left(\frac{\partial p}{\partial s}\right)_2$ opposite from the sign of $(p_c - p_2)$, the pressure is taken to be p_2. This makes the technique on those conical frustrums identical to the generalized shock expansion method. Reference 4 found this condition to occur on the nose of spherically blunted cones at $M_\infty \geq 3.0$ and also on the flares of blunted cone-flare bodies. The modifications made for bodies at an angle of attack are discussed below.

Results for blunted cones and blunted cones with flares were found to compare well with experimental data for $M_\infty \geq 3.0$. For the range $1.5 \leq M_\infty \leq 3$ the method predicted only part of the pressure over-expansion at the shoulder. However, this inaccuracy was found to have only a small effect on the force and moment coefficients.

New Modifications to the Second-Order Shock-Expansion Method

Two modifications are made here to the modified form of Jackson, et al.[4]. The approximate equation for the pressure gradient given by Equation (3) is compared to an "exact" pressure gradient downstream of a corner, and a new matching-point is determined for matching the second-order shock-expansion method with modified Newtonian theory on blunt-nosed bodies.

A. Derivation of "Exact" Pressure Gradient Downstream of a Corner

As mentioned above, the pressure gradient given by Equation (3) is only approximate. Therefore, an "exact" expression is derived here to compare with it. Although an "exact" expression is derived in Reference 13, it is not in a form comparable to Equation (3). For the analysis below, refer to Figure 3 for the nomenclature and geometry. Consider a surface streamtube as it passes around a corner. The stream surface (A) is close to the body surface, and the distance along a Mach line between the two stream surfaces is "a" (where a is very small). As the flow turns around the corner the distance "a" will increase because M increases and hence the distance between the stream surfaces will increase.

Define C_1 and C_2 as characteristics coordinates and s and n as coordinates along and normal to a streamline. At a corner only the C_1 family of characteristics (left-running characteristics) is present. The analytical development here is based on two equations from the method of characteristics[3]:

$$\frac{\partial p}{\partial C_1} = \cos \mu \left(\frac{\partial p}{\partial s} - \lambda \frac{\partial \delta}{\partial s} \right) \tag{7}$$

and

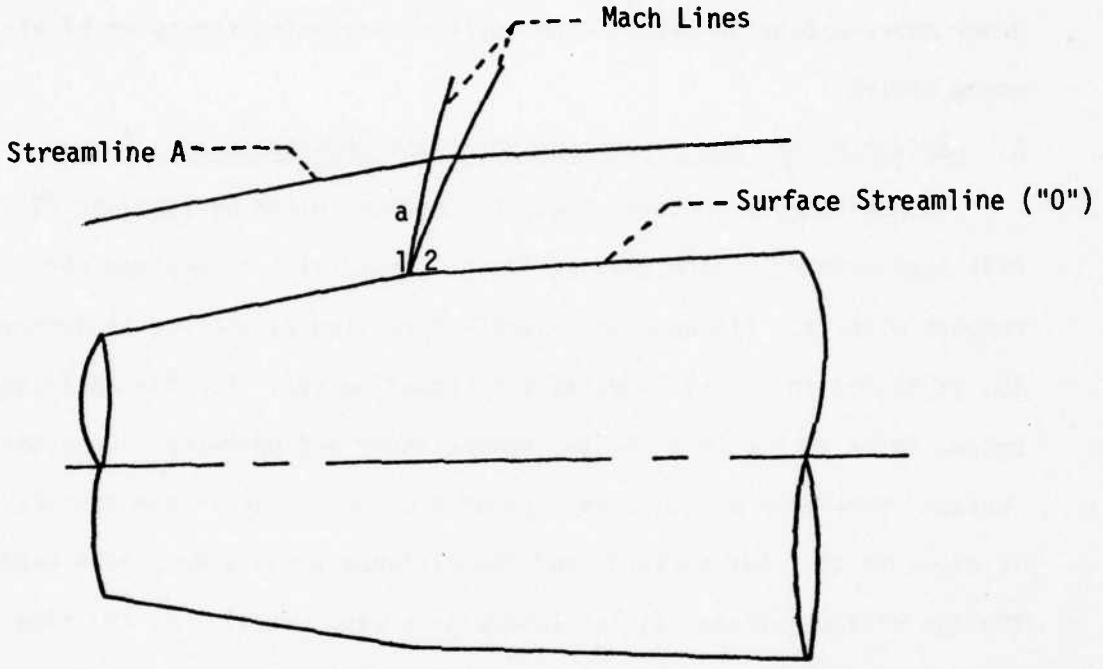

Figure 3. Flow About a Convex Corner on a Body of Revolution

$$\frac{\partial \delta}{\partial C_1} = \frac{-\sin \mu \sin \delta}{r} - \frac{\cos \mu}{\lambda} \left[\frac{\partial p}{\partial s} - \lambda \frac{\partial \delta}{\partial s} \right] \tag{8}$$

When Equation (7) is applied at the corner (on the surface), there results

$$\left(\frac{1}{\lambda} \frac{\partial p}{\partial s} - \frac{\partial \delta}{\partial s} \right)_o ds_o = \left(\frac{1}{\lambda \cos \mu} \frac{\partial p}{\partial C_1} \right)_o ds_o$$

where the subscript "o" refers to the surface streamline. Since $\frac{\partial p}{\partial C_1}$ is finite and the distance around the corner is zero, $ds_o = 0$ and the right side of the equation above is zero. The result is the Prandtl-Meyer expression

$$\frac{dp_o}{\lambda_o} = d\delta_o \tag{9}$$

and since $$d\nu_o = \frac{-dp_o}{\lambda_o} \tag{10}$$

Equation (9) integrates to

$$\nu_o - \nu_{o_1} = \delta_{o_1} - \delta_o \tag{11}$$

where the subscript "o_1" refers to the beginning of the expansion on the surface. Now consider the streamline off the surface, A. The pressure and deflection angle along streamline (A) can be represented by a Taylor series expansion about the surface streamline:

$$p_A = p_o + \left(\frac{\partial p}{\partial C_1} \right)_o a + \ldots \tag{12}$$

$$\delta_A = \delta_o + \left(\frac{\partial \delta}{\partial C_1} \right)_o a + \ldots \tag{13}$$

The partial derivatives are evaluated on the surface from Equations (7) and (8). Since the distance "a" changes with δ_o, it is convenient to

ratio it to its value when M = 1, a*. Then it can be related to Ω, the ratio of the one-dimensional cross-sectional area of the streamtube to that at M = 1, as follows:

$$\frac{a}{a^*} = \frac{2\pi ra}{2\pi ra^*} = \frac{\Omega}{\sin \mu} \tag{14}$$

Note that the thickness of the streamtube is a/sin μ and thus the cross-sectional area of the streamtube is $2\pi ra/\sin \mu$. Now substitute Equations (7), (8), and (14) into (12) and (13) to obtain

$$p_A = p_o + \lambda_o a_o^* \frac{Q_o}{2} + \ldots \tag{15}$$

and

$$\delta_A = \delta_o - a_o^* \left(\frac{\Omega_o \sin \delta_o}{r} + \frac{Q_o}{2} \right) + \ldots \tag{16}$$

where

$$Q_o \equiv \left(\frac{\Omega}{B} \right)_o \left[\frac{\partial p}{\partial s} - \lambda \frac{\partial \delta}{\partial s} \right]_o \tag{17}$$

Also, use the Taylor series expansion to write

$$\left(\frac{\partial p}{\partial C_1} \right)_A = \left(\frac{\partial p}{\partial C_1} \right)_o + \left(\frac{\partial^2 p}{\partial C_1^2} \right)_o a^* \left(\frac{a}{a^*} \right) + \ldots \tag{18}$$

$$\lambda_A = \lambda_o + \left[\left(\frac{\partial \lambda}{\partial p} \right)_{p_t} \frac{\partial p}{\partial C_1} + \left(\frac{\partial \lambda}{\partial p_t} \right)_p \frac{\partial p_t}{\partial C_1} \right]_o a^* \left(\frac{a}{a^*} \right) + \ldots \tag{19}$$

$$\cos \mu_A = \cos \mu_o + \left(\frac{\partial \cos \mu}{\partial C_1} \right)_o a^* \left(\frac{a}{a^*} \right) + \ldots \tag{20}$$

Appendix A shows that the differential distance along streamline (A) is given by

$$\frac{ds_A}{d\delta_o} = -a^* \left(\frac{a}{a^*}\right) \left(\frac{\gamma+1}{2}\right) \frac{M_o^3}{(M_o^2-1)} \tag{21}$$

Substitute Equations (9) and (15) through (21) into Equation (7) applied along streamline A. The following equation then results:

$$\frac{d}{d\delta_o} \left[Q + \frac{\Omega \sin \delta}{r}\right]_o = - \left(\frac{\gamma+1}{4}\right) \frac{M_o^4 Q_o}{(M_o^2-1)^{3/2}} \tag{22}$$

This equation can be integrated numerically around the corner along with the Prandtl-Meyer equation to determine Q_o, and using Equation (17) the pressure gradient $\left(\frac{\partial p}{\partial s}\right)_o$ is obtained from Q_o.

It should be noted that Equation (22) neglects the total pressure derivative $\frac{\partial p_t}{\partial C_1}$ in Equation (19). As noted in Reference 3, this term is generally negligible. To be certain that it is, the accuracy of neglecting this term will be determined during the next year of this project.

Figure 4 compares the pressure gradient parameter $\frac{r}{p_\infty} \frac{\partial p}{\partial C_1}$, calculated from the approximate method, Equation (3), and the "exact" method, Equation (22). The pressure gradient is presented for different deflection angles downstream of the corner of an initial cone with a 9° half angle for M_∞ = 2.5 and 5. This figure shows that errors in the pressure gradient parameter as high as 35% occur for M_∞ = 2.5, and this maximum error drops to about 27% at M_∞ = 5. In both cases the "exact" values

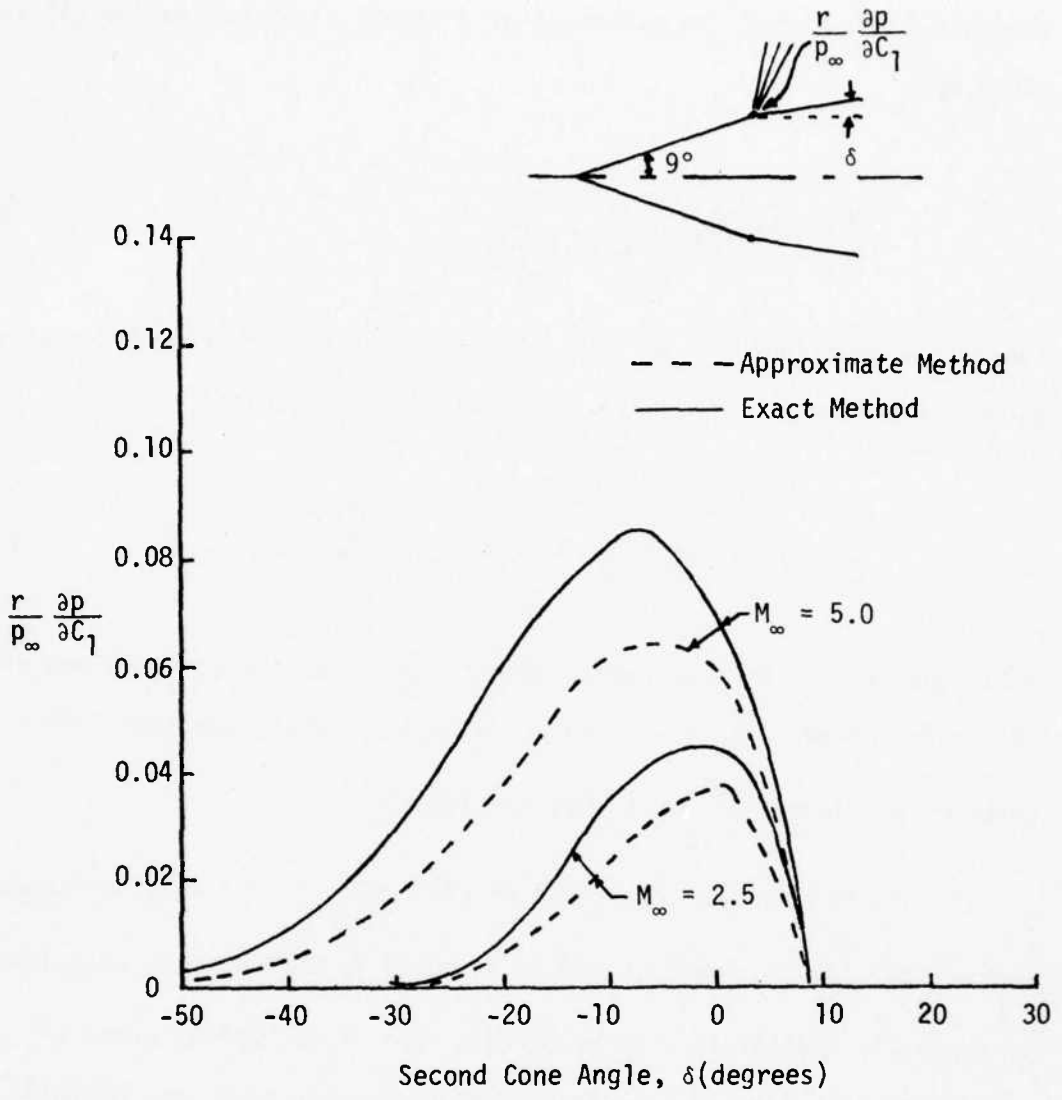

Figure 4. Pressure Gradient at Corner of Biconics, Initial Cone Angle = 9°

are larger than the approximate values. Figure 5 gives $\frac{r}{p_\infty}\frac{\partial p}{\partial C_1}$ as a function of deflection angle downstream of a 40° half-angle cone. At $M_\infty = 2.5$ the error is about 40% at $\delta = 14°$. The curve for $M_\infty = 5$ has a different feature in that $\frac{r}{p_\infty}\frac{\partial p}{\partial C_1} < 0$ for $11° \leq \delta < 40°$, and errors up to about 25% occur. Figures 4 and 5 illustrate that large errors can occur when using the approximate relation for the pressure gradient. Note that since the initial body surfaces are cones with attached shock waves, $\partial p_t/\partial C_1 = 0$ and Equation (22) is the appropriate "exact" relation for these figures.

For slender bodies, the effect of using the exact pressure gradient rather than the approximate relation is small. Figure 6 compares the results from both techniques with the pressure distribution from Solomon, et al[7] for a pointed ogive with a boattail. The "exact" pressure gradient method gave slightly better results for the boattail, but otherwise both methods were very close. This same statement cannot be made for thick bodies.

B. New Matching Point for Blunted Bodies

The location of the point used to match modified Newtonian theory to the second-order shock-expansion method has a large effect on the accuracy of predicting the over-expansion on blunted cones at the lower supersonic Mach numbers. As mentioned above, Jackson, et al[4] used the position where the body slope is the same as the maximum wedge angle for an attached shock wave. They found that this location predicted part of the over-expansion at the shoulder. The results compared well with experimental data at $2.30 \leq M_\infty \leq 4.63$, where the over-expansion is small, but the comparison was poor at $M_\infty = 1.5$, where the over-expansion is large. Although the work statement in the present contract called for a method

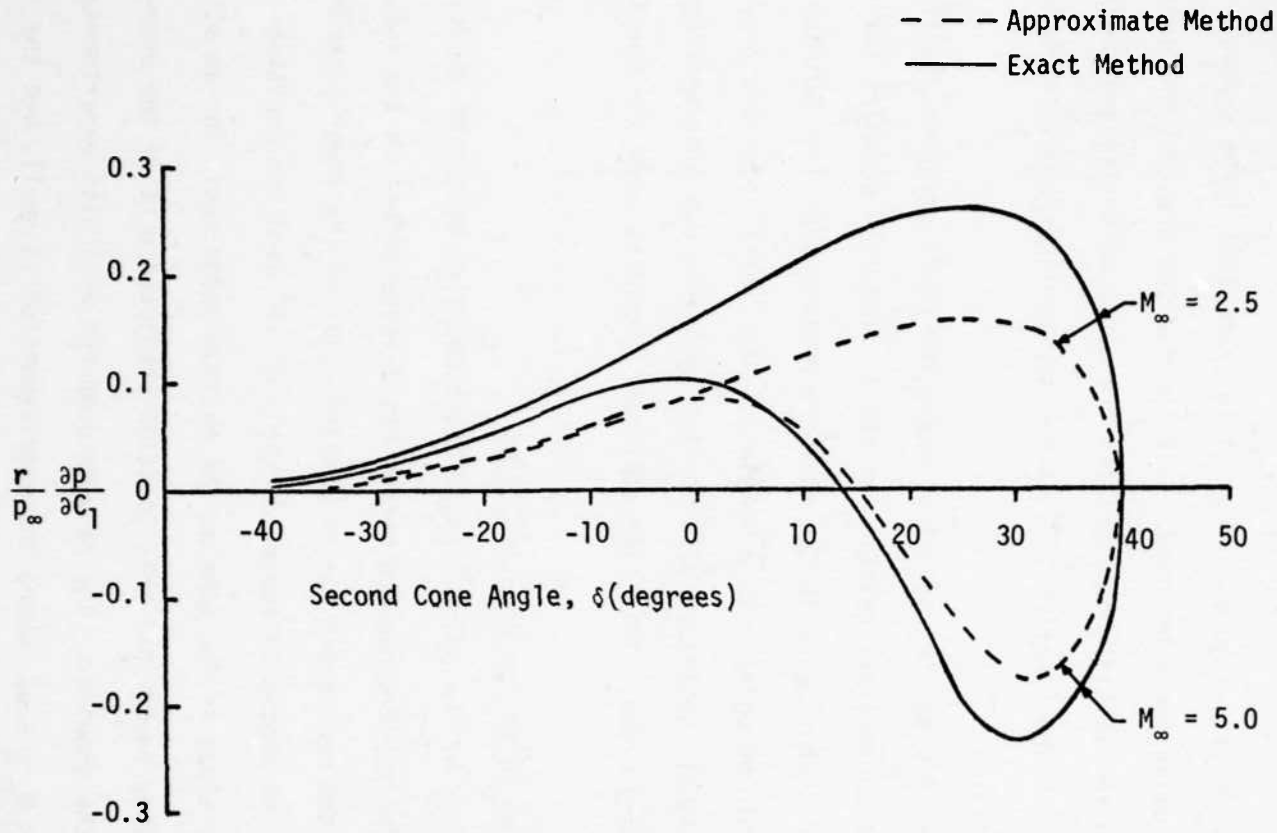

Figure 5. Pressure Gradient at Corner of Biconics, Initial Cone Angle = 40°

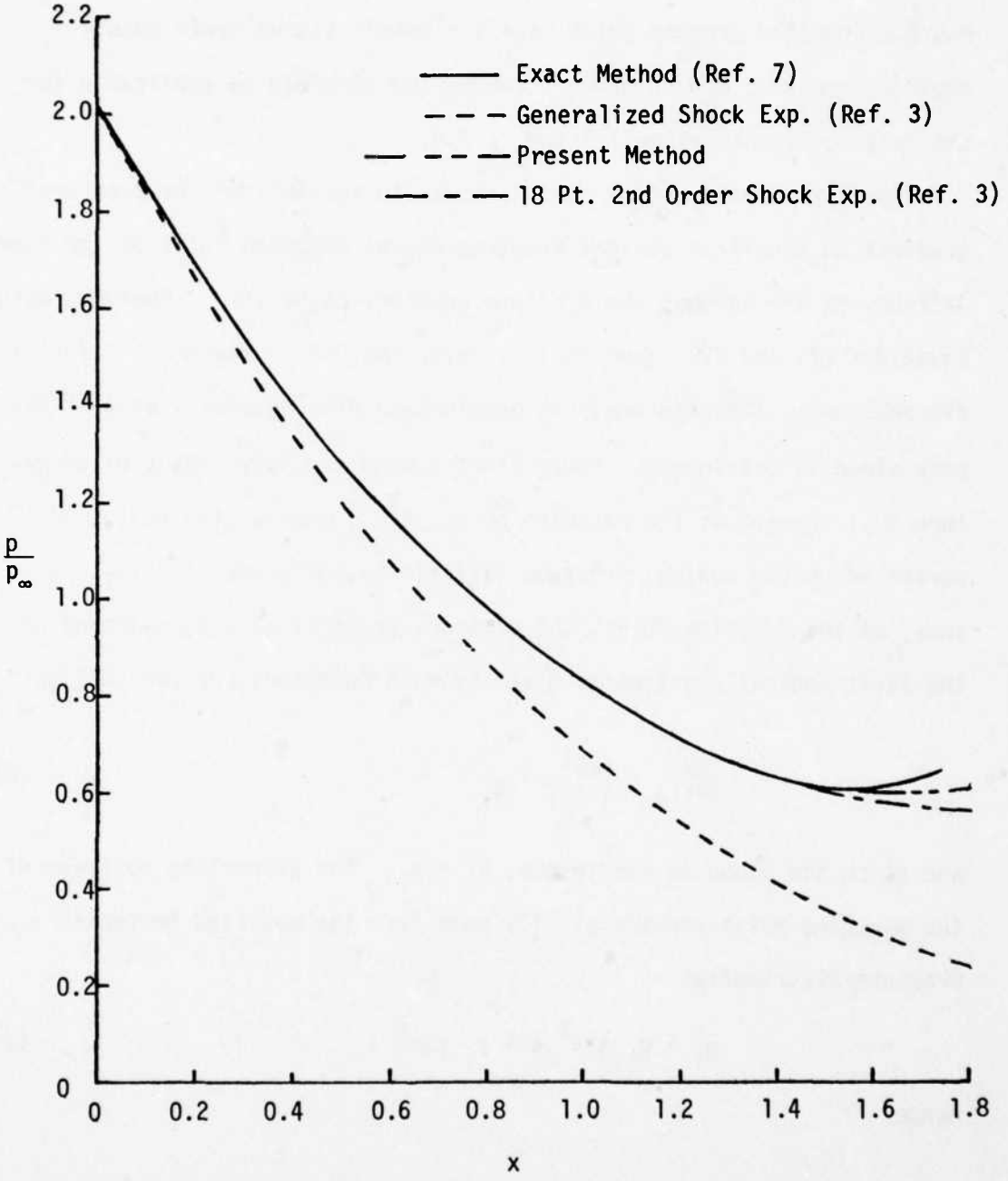

Figure 6. Pressure Distribution on Body Shape
$r=(15+2x-x^2)^{1/2} - \sqrt{15}$, $M_\infty=3$

applicable to the $2.5 \leq M_\infty \leq 6.0$ range, it was agreed to try to extend it down to $M_\infty \approx 1.2$. If this could be done, then the subroutine of Moore's computer program which used Van Dyke's second order theory could be replaced by the present method and it would be applicable for the full supersonic range $1.2 \leq M_\infty \leq 6.0$.

The first modification made here was to account for the pressure gradient on the first conical frustrum at the matching point on the nose. Jackson, et al[4] assumed the pressure gradient to be zero. However, both Equations (3) and (22) show that whenever the body curvature $(-\partial\delta/\partial s)$ is discontinuous, then the pressure gradient is discontinuous, even if the body slope is continuous. For a blunted nose the body radius of curvature just forward of the matching point is R_1, whereas the radius of curvature on the conical frustrum is infinite and hence $(\partial\delta/\partial s)_2 = 0$. Thus, at the matching point, the pressure gradient at the beginning of the first conical frustrum is given by both Equations (3) and (22) as

$$\left(\frac{\partial p}{\partial s}\right)_2 = \left(\frac{\partial p}{\partial s}\right)_1 + \frac{\lambda_1}{R_1} \tag{23}$$

and since the slope is continuous, $p_2 = p_1$. The properties upstream of the matching point (subscript "1") come from the modified Newtonian pressure distribution

$$p_1 = p_t \sin^2 \delta + p \cos^2 \delta \tag{24}$$

Hence

$$\left(\frac{\partial p}{\partial s}\right)_1 = \frac{-1}{R_1}\left(\frac{\partial p}{\partial \delta}\right)_1 = \frac{-2 \sin \delta_1 \cos \delta_1 (p_t - p_\infty)}{R_1} \tag{25}$$

where R_1 is the radius of curvature at the matching point.

The pressure distribution downstream of the matching point can now be calculated by the second-order shock-expansion method. Equation (23) gives the pressure gradient on the first conical frustrum (which is tangent to the nose at the matching point). A tangent body is then transcribed about the remaining body and the technique described previously can be applied. Note, however, that the pressure gradient at each corner is calculated from the "exact" expression given by Equation (22).

It was found that the matching point used by Jackson, et al[4] was not the best one when the pressure gradient is used on the first conical frustrum. Figures 7 and 8 show the pressure distribution over a sphere computed with three different matching points (M = 1.1, 1.2, and 1.4) for M_∞ = 5 and 3.5. The results are compared with "exact" inviscid calculations[14]. The pressure distributions with matching points at M = 1.2 and 1.4 are very close. Although the distribution for the matching point at M = 1.1 differs initially from the other two, it blends into the other two solutions downstream of the matching point. For the lower supersonic range, Figure 9 gives the distribution of the pressure coefficient over a sphere with matching points at M = 1.1, 1.15, and 1.2 for M_∞ = 1.5. The results are compared with experimental data[15]. Here the location of the matching point is more critical than that in Figures 7 and 8. It is also evident that the modified Newtonian pressure coefficient is not very accurate near the matching points. Although an optimum matching point cannot be determined from Figures 7 through 9, it appears that it lies in the range $1.1 < M < 1.2$. Further investigation is needed to define it more accurately as a function of M_∞. Presently the matching point is calculated as the position on the nose where the modified Newtonian pressure distribution gives a local Mach number of 1.15.

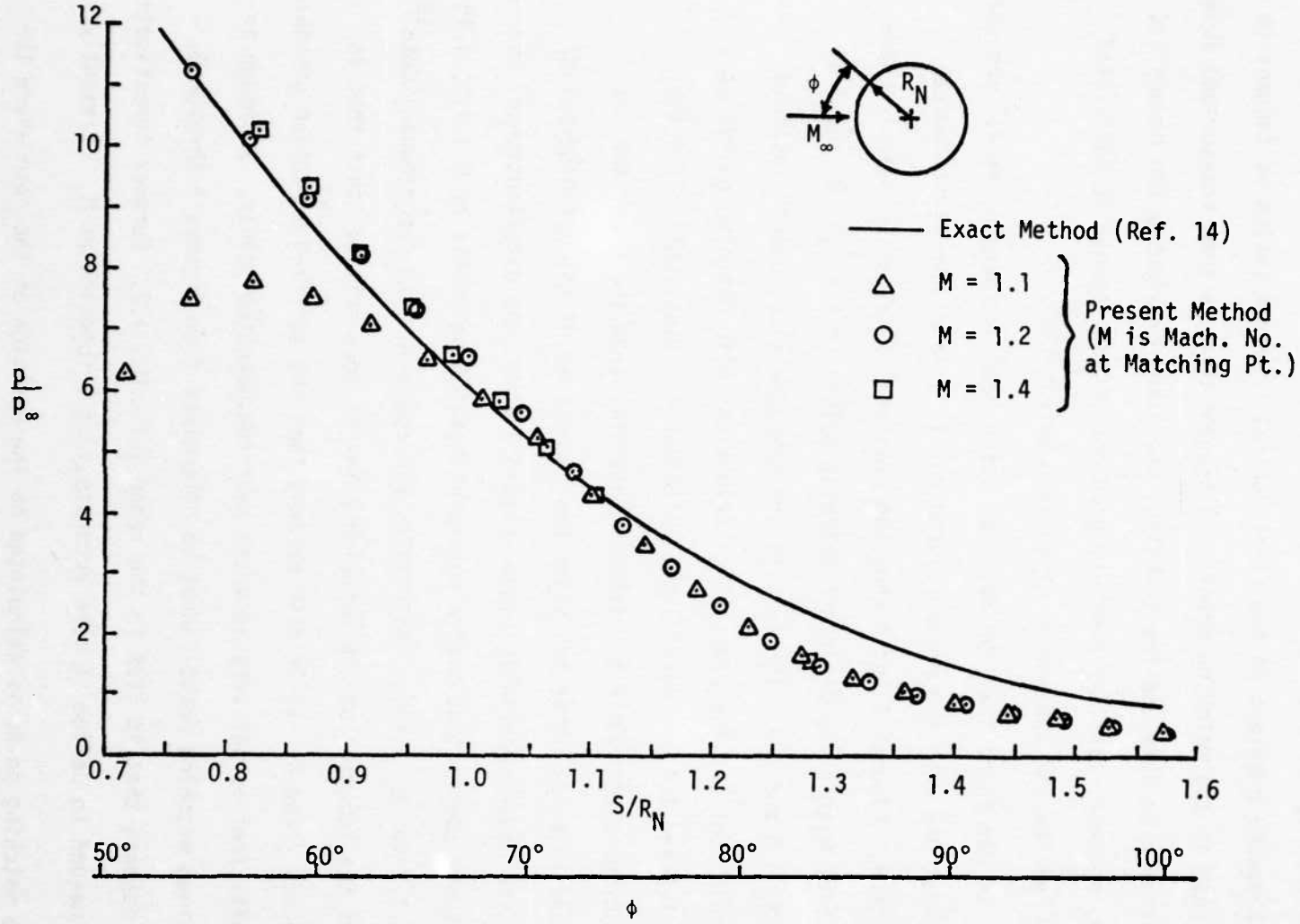

Figure 7. Pressure Distribution on Sphere, M_∞=5.0

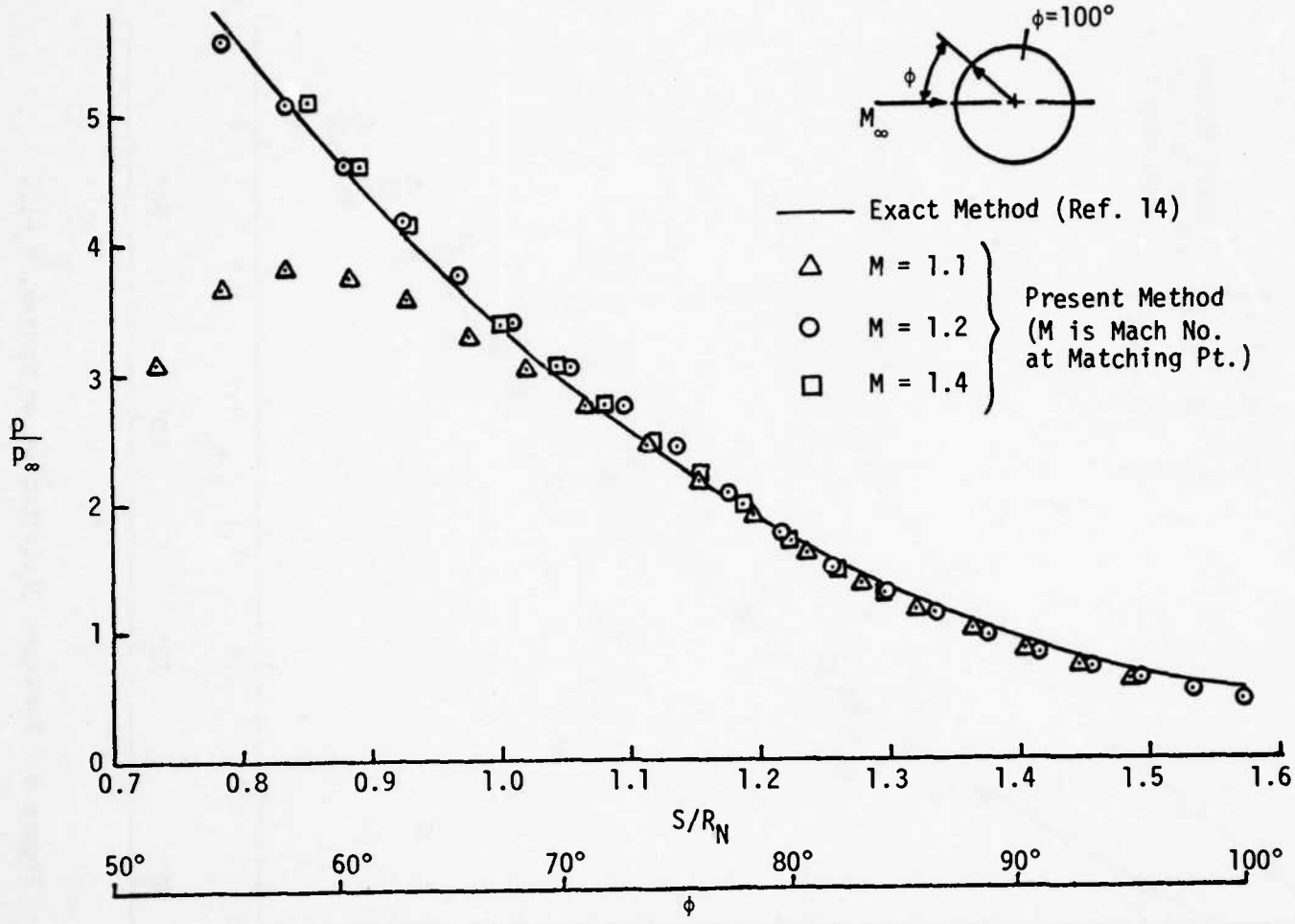

Figure 8. Pressure Distribution on Sphere, M_∞=3.5

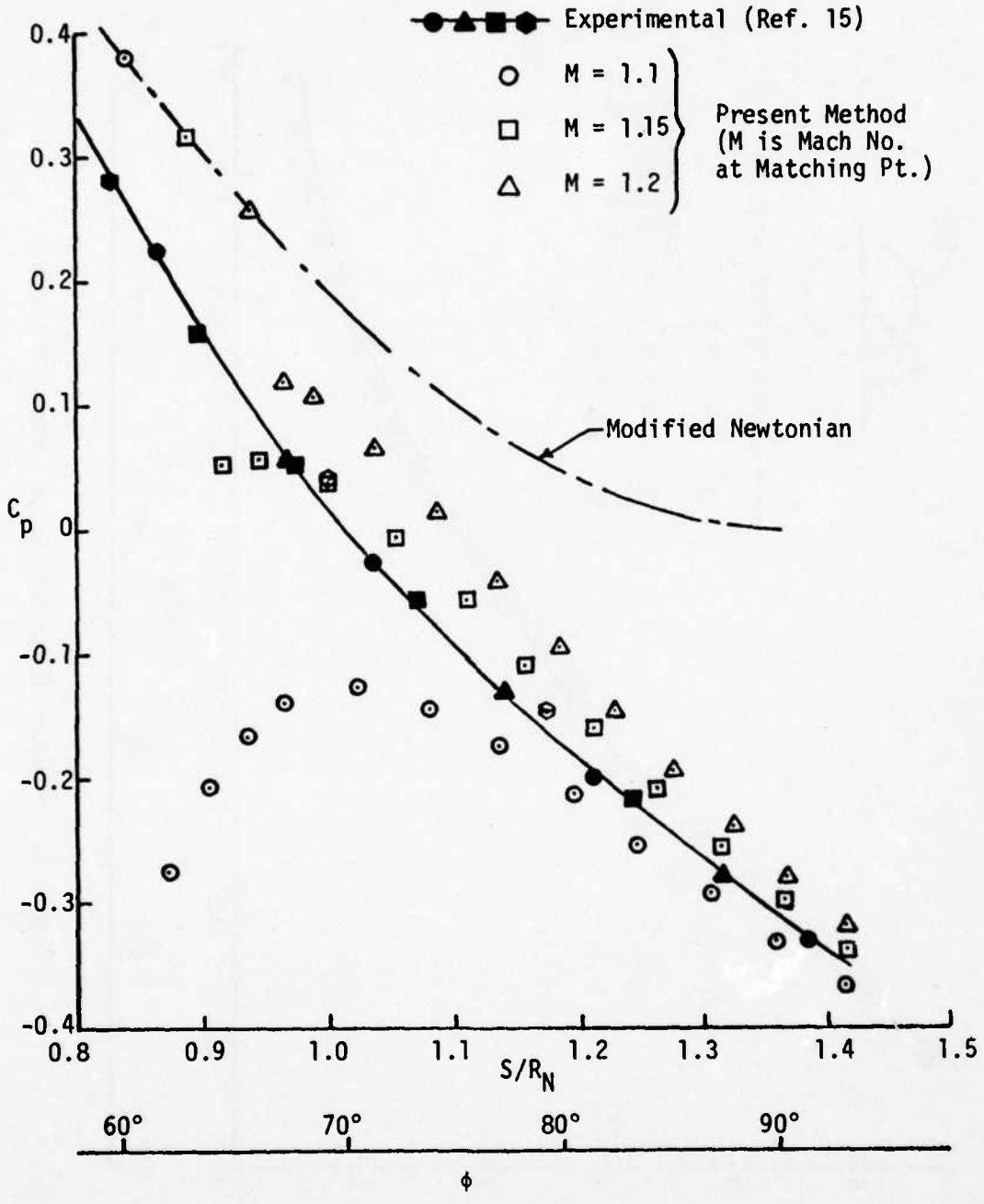

Figure 9. Pressure Distribution on Sphere, M_∞=1.5

Method for Predicting Pressure Distribution at $\alpha > 0$

An accurate calculation of surface pressures on bodies of revolution at $\alpha > 0$ is much more complicated than that for the body at $\alpha = 0$. At $\alpha = 0$ the meridian lines on the surface are also surface streamlines. However, at incidence the streamlines wrap around the body and no longer follow the meridian lines. If the shape of a streamline can be determined approximately, then an equivalent body of revolution can be generated for that streamline and the method described for $\alpha = 0$ can be used to calculate the pressure distribution along this equivalent body of revolution representing the streamline. Several streamlines must be used in order to get the circumferential pressure distribution along the actual body.

Jackson, et al[4] assumed that the surface streamlines in the windward and leeward planes of symmetry could be approximated by the body shape obtained by transforming the body-axis coordinate into wind-axis coordinates. This transformation is obtained by rotating the body-axis coordinate system in the plane of symmetry clockwise through the angle α with the center of rotation at the center of the spherical cap, as shown in Figure 10. The windward ($\theta = -90°$) and leeward ($\theta = 90°$) streamlines are transformed into the equivalent bodies of revolution represented by the body coordinates in the wind-axis system. (See Figure 11). On the other hand, the streamline for $\theta = 0°$ is approximated by the body-axis coordinates of a meridian of the true body shape. The equivalent body of revolution for this streamline is, therefore, the same as the true body at $\alpha = 0$. Between $\theta = \pm 90°$ and $\theta = 0°$, the streamlines for each radial angle θ of interest are assumed to follow the equivalent bodies of revolution represented by

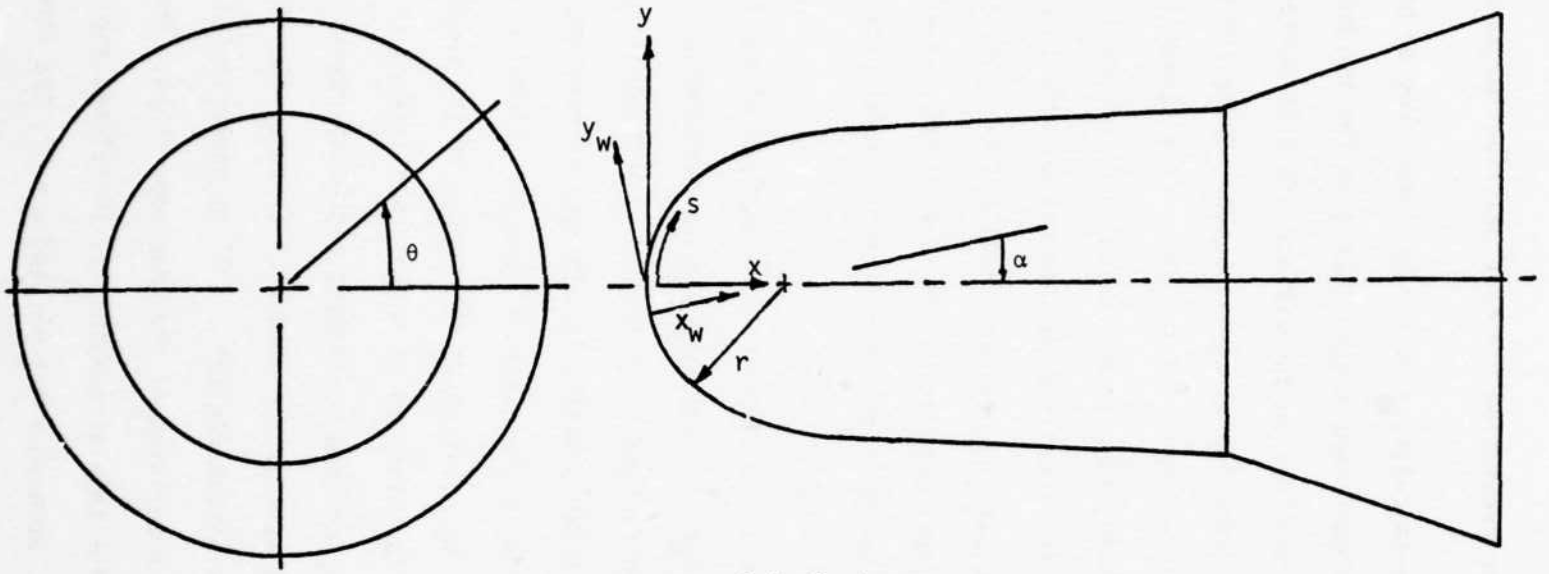

Figure 10. Axis Systems

$$X_w = (R_n - x)(1-\cos\alpha)\sqrt{1-\cos^2\sigma} + y\sin\alpha\sin\sigma + x \tag{26}$$

$$Y_w = -y(1-\cos\alpha)\sqrt{1-\cos^2\sigma} + (R_n - x)\sin\alpha\sin\sigma + y \tag{27}$$

Figure 11 illustrates these equivalent bodies of revolution representing the streamlines. As noted in Reference 4, this approximation requires α to be small enough for the stagnation point to remain on the spherical cap, and also α must be small enough for the coordinates of the equivalent body in the leeward plane ($\theta = 90°$) to remain positive.

For the analysis here, it was decided to modify the technique described above for $-90° < \theta < 90°$, but use the same technique for the windward ($\theta = -90°$) and leeward ($\theta = 90°$) planes of symmetry. One reason for the modification is that for $-90° < \theta < 90°$ the stagnation point on the equivalent bodies of revolution do not correspond to that on the true body. For example, at $\theta = 0$, Equations (26) and (27) place the stagnation point at the nose ($x = 0$, $y = 0$) of the actual body instead of its actual location for $\alpha > 0$. Therefore, the method used herein is to assume that the streamlines on the spherical cap follow the meridian lines of the sphere in the wind-axis system up to the sphere-cone juncture. For the region downstream of this juncture, the streamlines are assumed to follow the meridian lines in the body-axis system. Although the approach used here downstream of the sphere-cone juncture is also an approximate method, the streamlines on the spherical cap are the correct ones up to the sonic point.

The cone pressure used in Equation (1) by Jackson, et al[4] on each conical frustrum was the tangent cone pressure. For an axisymmetric body at $\alpha > 0$, the tangent cone is an equivalent cone whose slope is

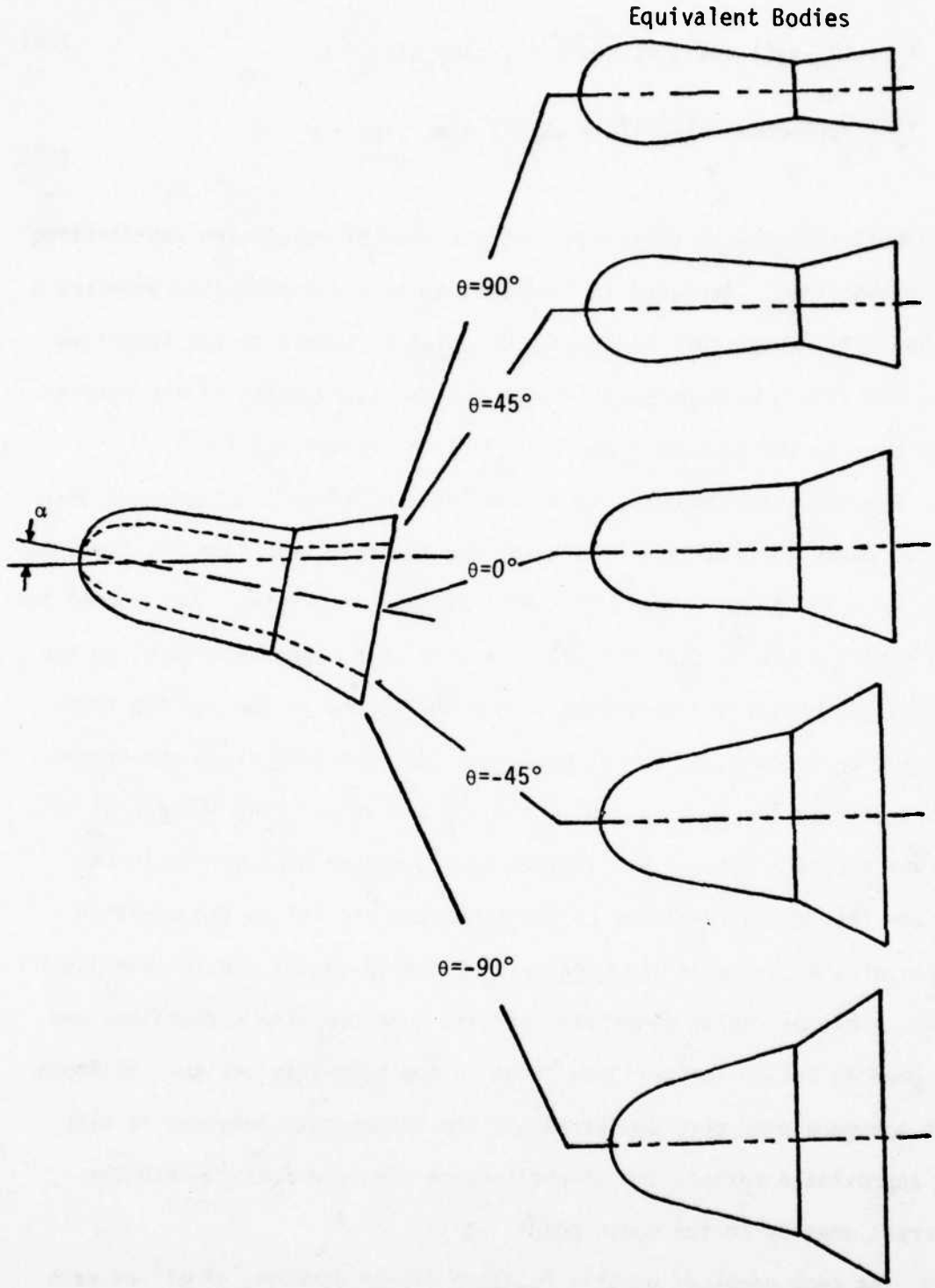

Figure 11. Typical Equivalent Body Shapes from Ref. 4

the same as the slope of the actual conical frustrum with respect to the wind axis system. The equivalent cone angle δ_{eq} corresponding to a cone angle δ is given by

$$\sin \delta_{eq} = \cos \alpha \sin \delta - \sin \alpha \cos \delta \sin \theta \tag{28}$$

It was found, however, that even for a pointed cone at $\alpha > 0$, the tangent cone pressure differed from the actual pressure, particularly at the lower supersonic Mach numbers. In order to get a more accurate pressure on the tangent cone at $\alpha > 0$, the tangent cone pressure was replaced by the following relation:

$$\frac{p_c}{p_\infty} - \left(\frac{p_c}{p_\infty}\right)_{\alpha=0} = \left(\frac{p}{p_\infty}\right)_{MN} - \left(\frac{p}{p_\infty}\right)_{MN,\alpha=0}$$

The second term on the left is the cone pressure at $\alpha = 0$ whereas the two terms on the right are the modified Newtonian pressures at $\alpha > 0$ and $\alpha = 0$, respectively. This equation gives the change in cone pressure with α as the change in modified Newtonian pressure with α. Since the modified Newtonian pressure is given by

$$\left(\frac{p}{p_\infty}\right)_{MN} = \left(\frac{p_t}{p_\infty} - 1\right) \sin^2 \delta_{eq} + 1$$

and $\delta_{eq} = \delta$ at $\alpha = 0$, then the pressure on the tangent cone at $\alpha > 0$ becomes

$$\frac{p_c}{p_\infty} = \left(\frac{p_c}{p_\infty}\right)_{\alpha=0} + \left(\frac{p_t}{p_\infty} - 1\right) \left(\sin^2 \delta_{eq} - \sin^2 \delta\right) \tag{29}$$

To test the accuracy of Equation (29), comparisons were made with "exact" numerical calculations[14] and experimental data[15]. Figure 12 shows the circumferential pressure variation on a pointed 5° cone at $M_\infty = 3.5$ for $\alpha = 0$, 5°, and 10°. At $\alpha = 10°$ the tangent cone method overpredicts the pressure about 15%, whereas Equation (29) is less than 1% above the "exact" calculation. Figure 13 compares the circumferential pressure coefficient determined from Equation (29) to experimental data for a 9° cone at $\alpha = 12°$ with $M_\infty = 1.9$. In the windward plane the tangent cone method overpredicts p/p_∞ by 20% while Equation (29) underpredicts it by 3%. Figure 14 compares the present theory and tangent cone method with "exact" numerical results in the windward plane for a 9° cone at $M_\infty = 3.5$ for $0 \leq \alpha \leq 10°$. Here, also, Equation (29) was found to give better results than the tangent cone method. As the Mach number increases, the difference between the results from the two methods decrease. This fact is illustrated in Figure 15 for a 20° cone at $M_\infty = 10$ for $\alpha = 1°$, 5°, and 10°.

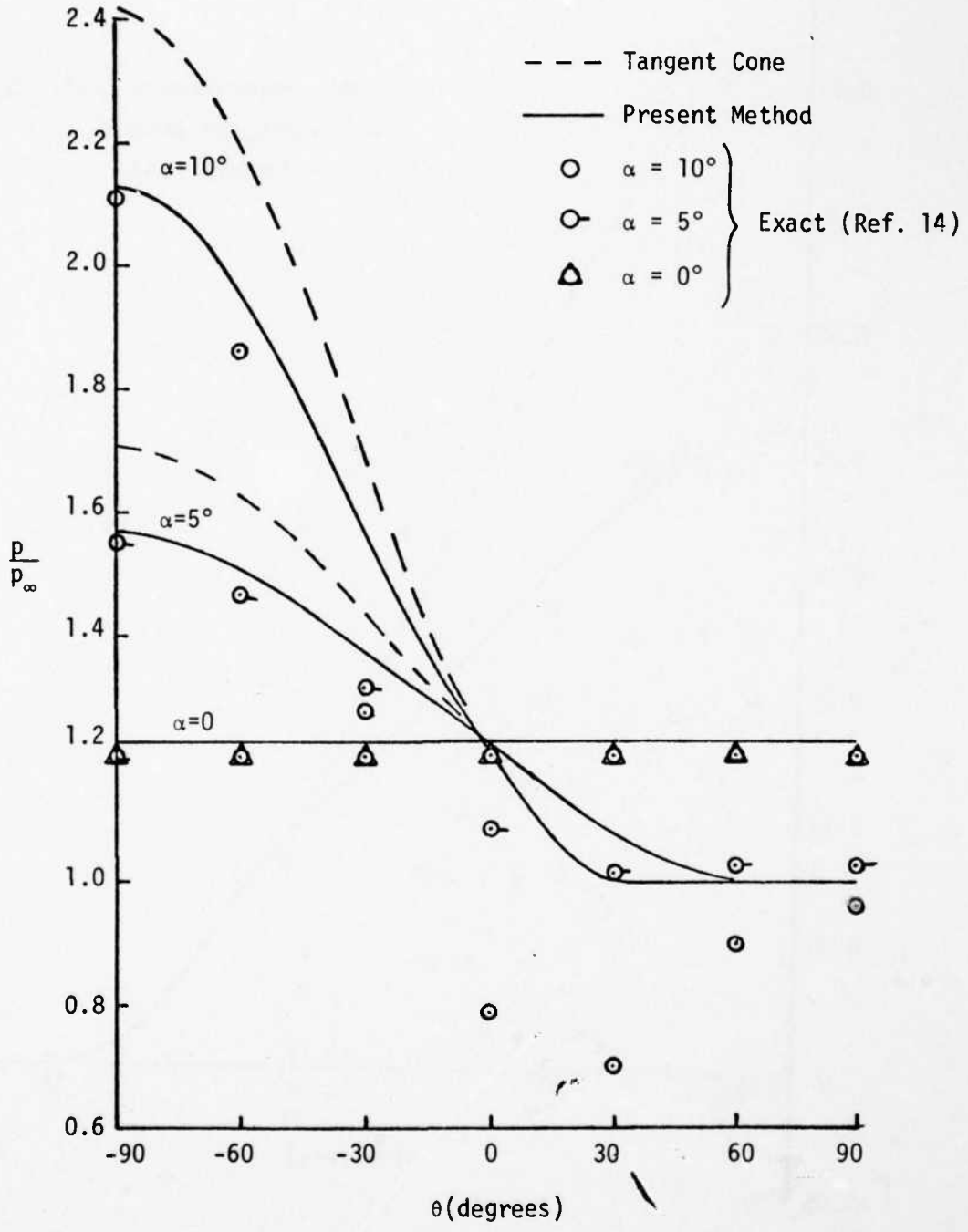

Figure 12. Circumferential Pressure Distribution Around Pointed 5° Cone, M_∞=3.5, α=10°, 5°, 0°

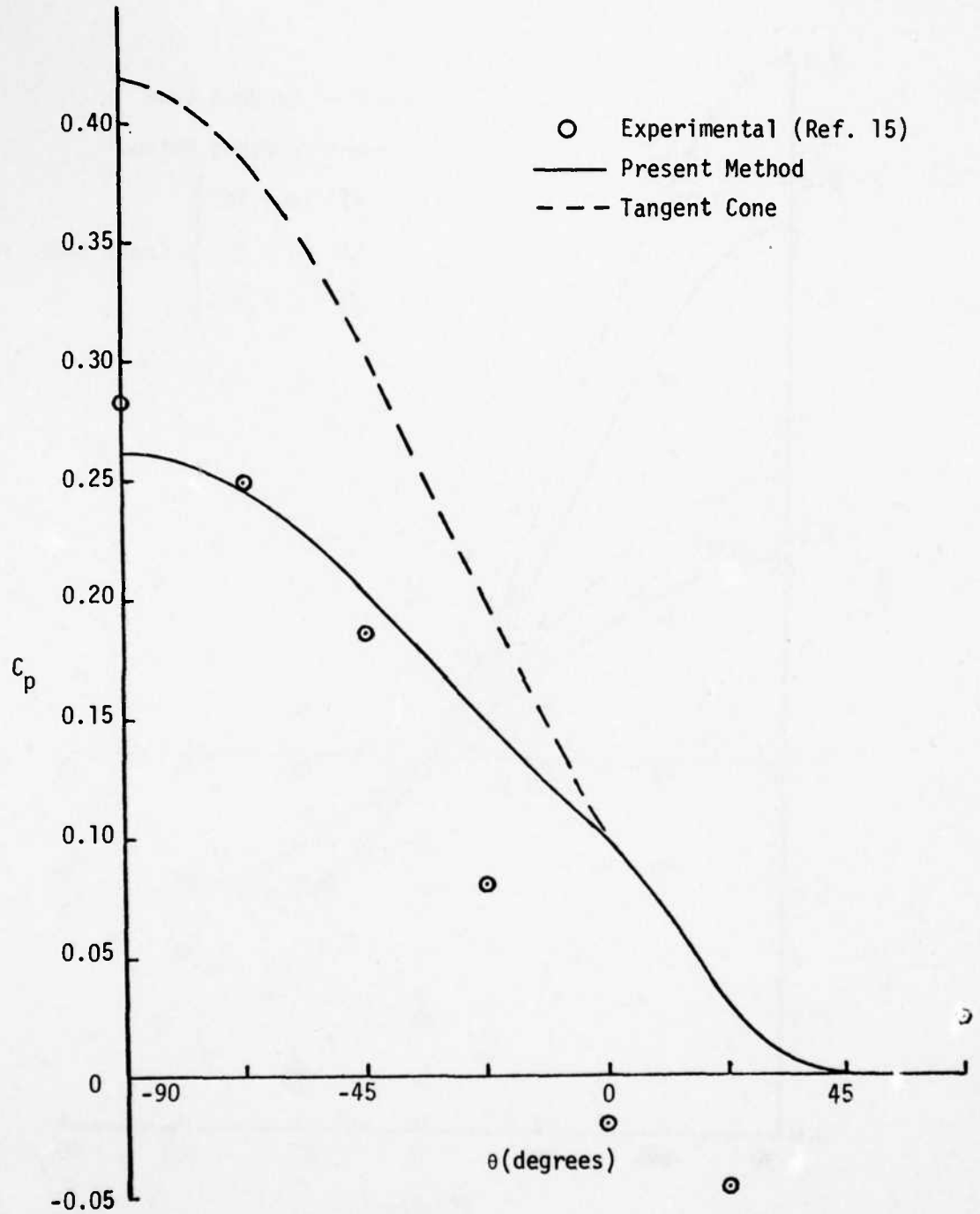

Figure 13. Circumferential Pressure Distribution Around Pointed 9° Cone, M_∞=1.9, α=12°

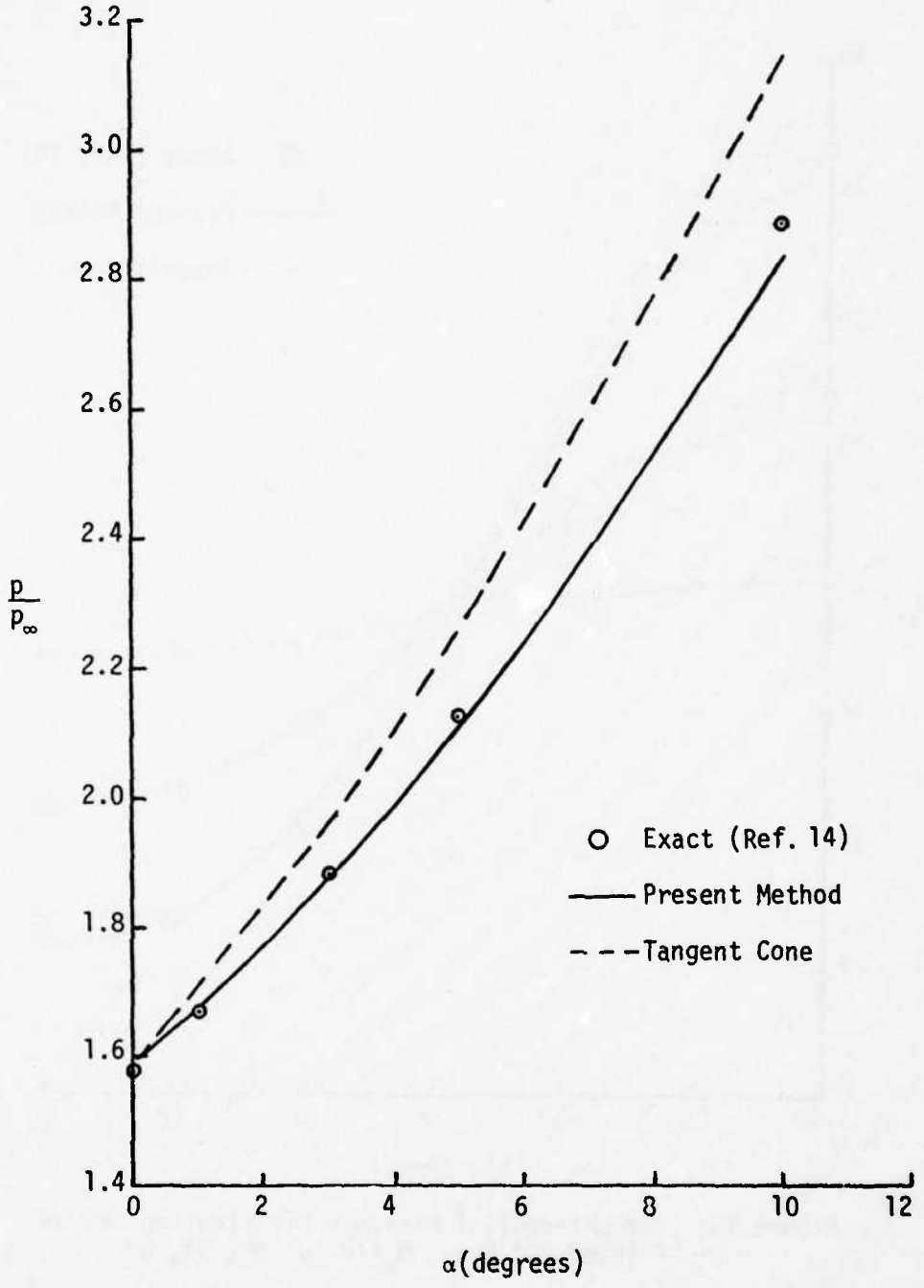

Figure 14. Pressure Distribution in Windward Plane of 9° Cone, M_∞=3.5

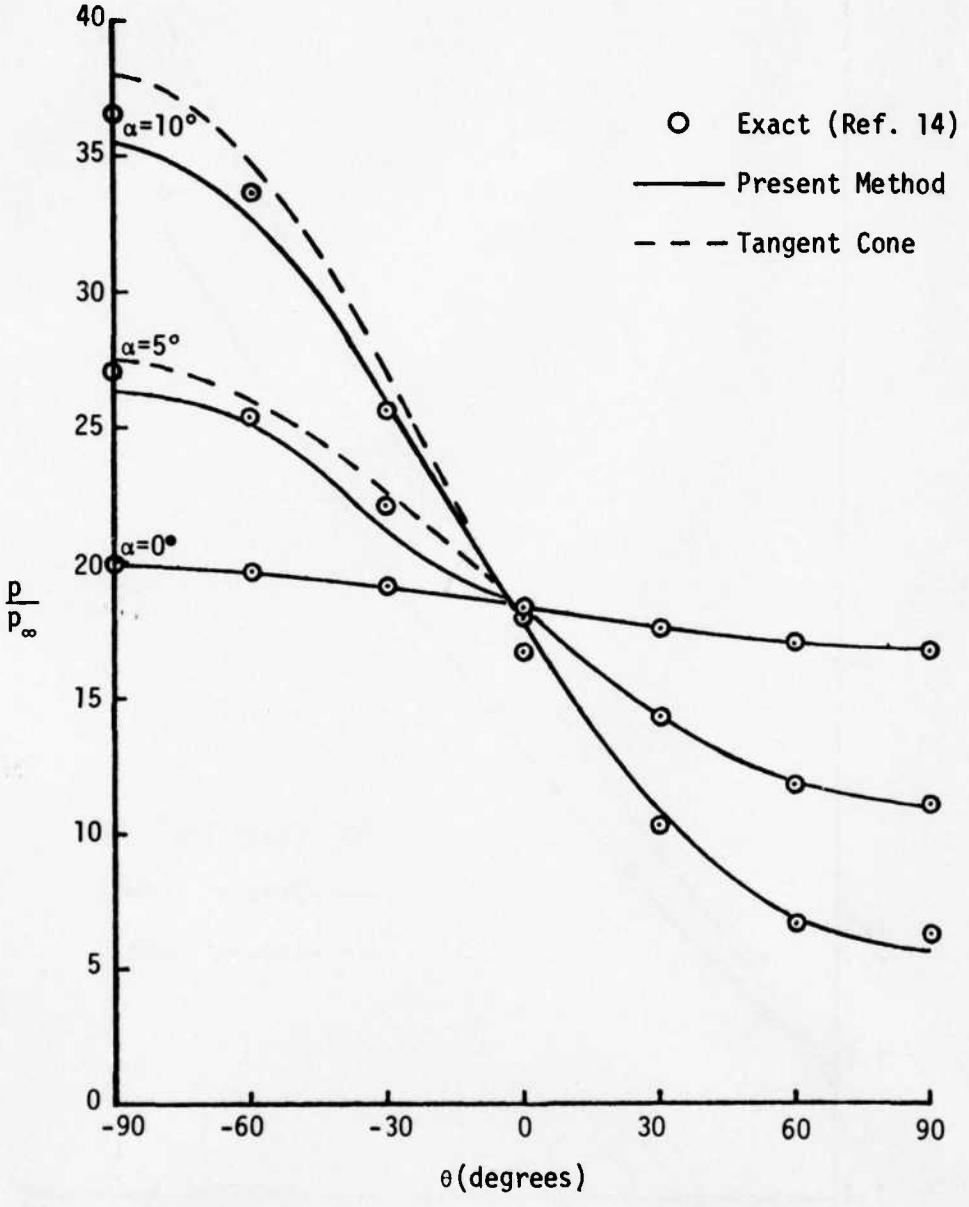

Figure 15. Circumferential Pressure Distribution Around Pointed 20° Cone, M_∞=10, α=10°, 5°, 0°

RESULTS AND DISCUSSION

The pressure distribution and force and moment coefficients have been calculated and compared with experimental data for blunted cones and blunted cones with a flared afterbody. Two of these bodies, called Model 1 and Model 2, are illustrated in Figure 16.

Blunted Cones

Pressure distributions over Model 1, a spherically blunted 11.5° cone, at $\alpha = 0$ are shown in Figures 17, 18, 19, and 20 for $M_\infty = 1.5$, 1.9, 2.3, and 4.63, respectively. The results from the present method are compared with that of Jackson, et al[4] and experimental data[4]. Figure 17 and 18 indicate the capability of the present method to calculate the pressure over-expansion near the shoulder much better than Jackson's method. As M_∞ increases the over-expansion decreases, and at $M_\infty = 4.63$ it vanishes.

Figure 21 compares the calculated pressure distribution with experimental data[15] on a spherically blunted 9° cone at $\alpha = 0$ and $M_\infty = 1.5$. Two numerical solutions are presented, one with a matching point at $M = 1.10$ and the other at $M = 1.15$. The over-expansion here is significant, and the results for $M = 1.10$ are very close to the experimental data. Figures 22 and 23 give results for the same body at $M_\infty = 1.9$ and 4.63, respectively. The agreement with experiment is good here also, and the over-expansion is not present in Figure 23. The "hook" in the calculated pressure distribution at the matching point is the same as that observed in Figures 7, 8, and 9.

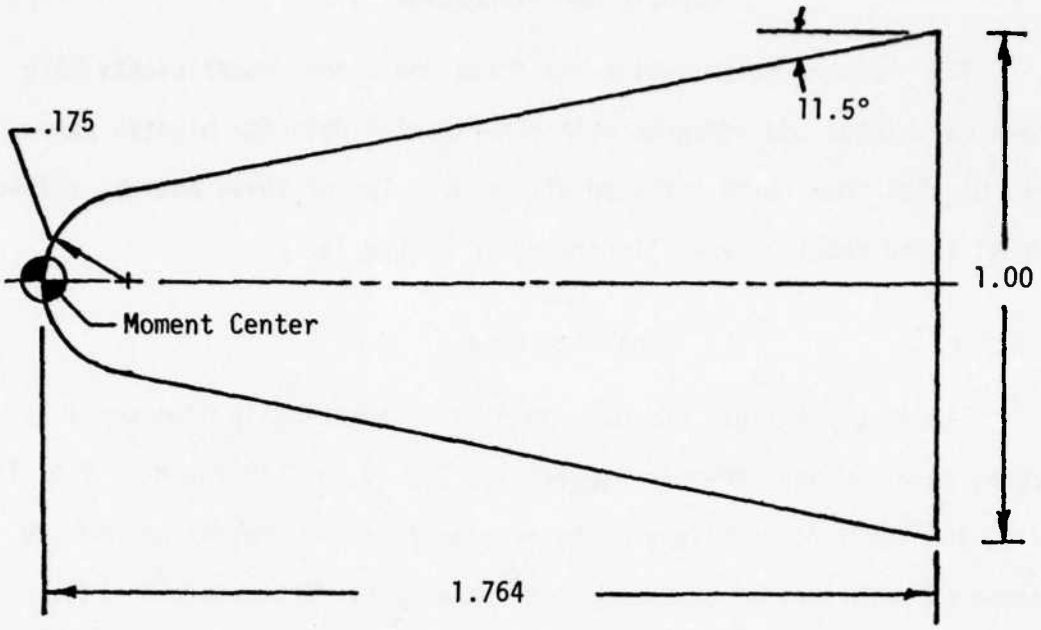

Model 1; d=0.572 ft (0.174m)

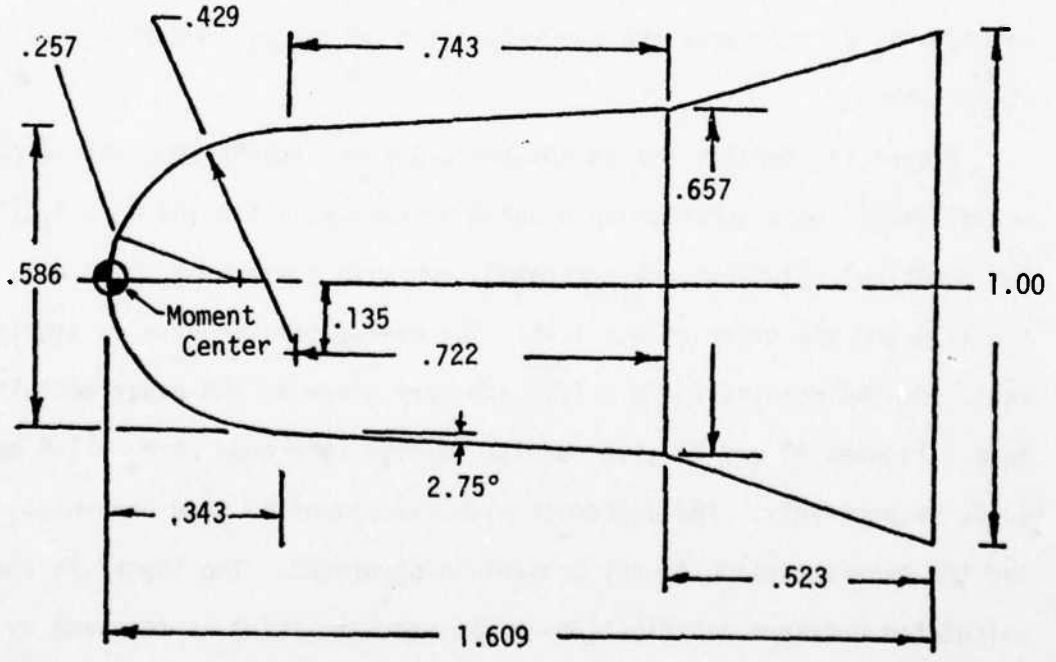

Model 2; d=0.583 ft (0.178 m)

Figure 16. Model Details (All Dimensions are Relative to Base Diameter)

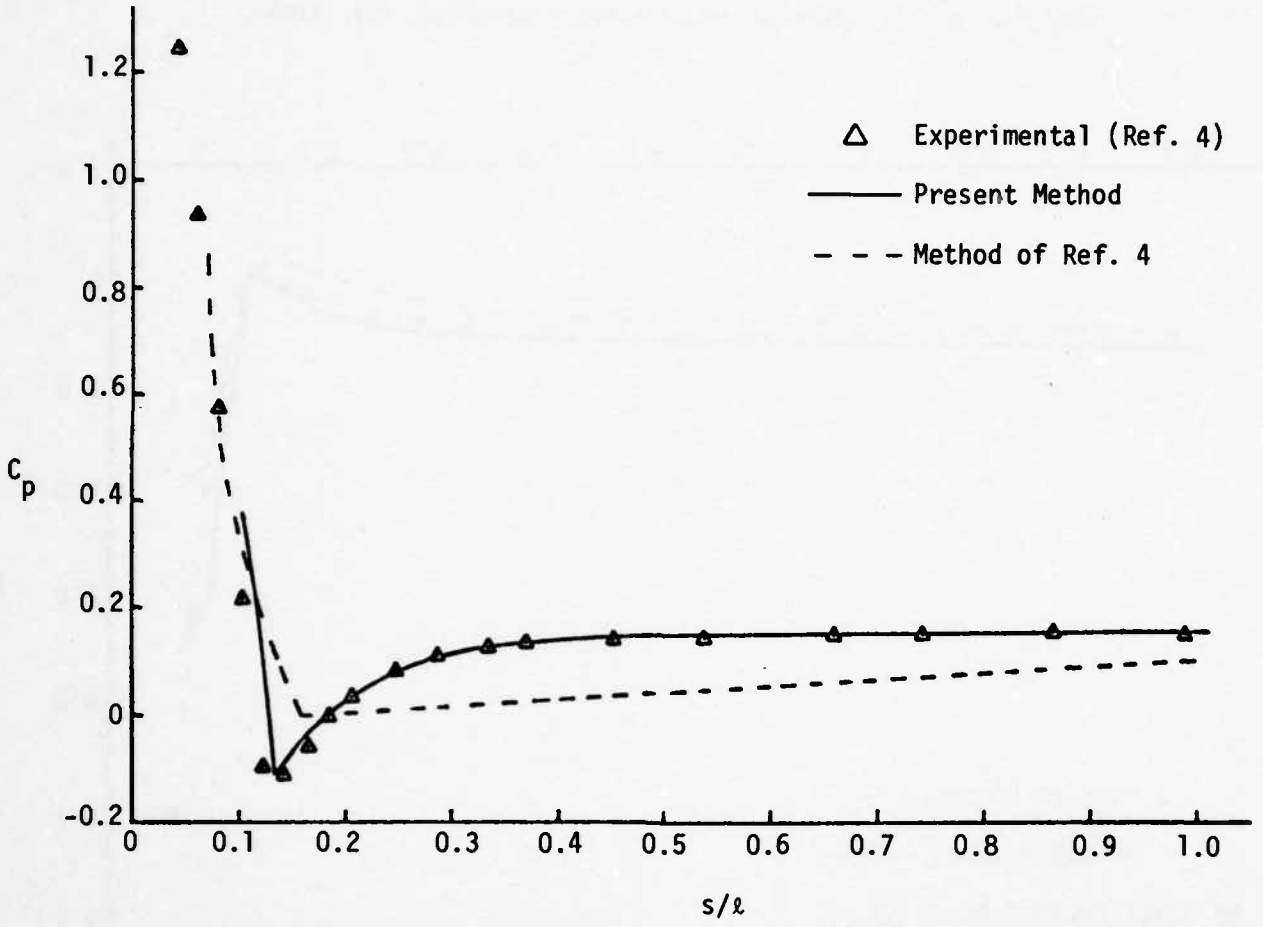

Figure 17. Pressure Distribution on Model 1, M_∞=1.5,α =0°

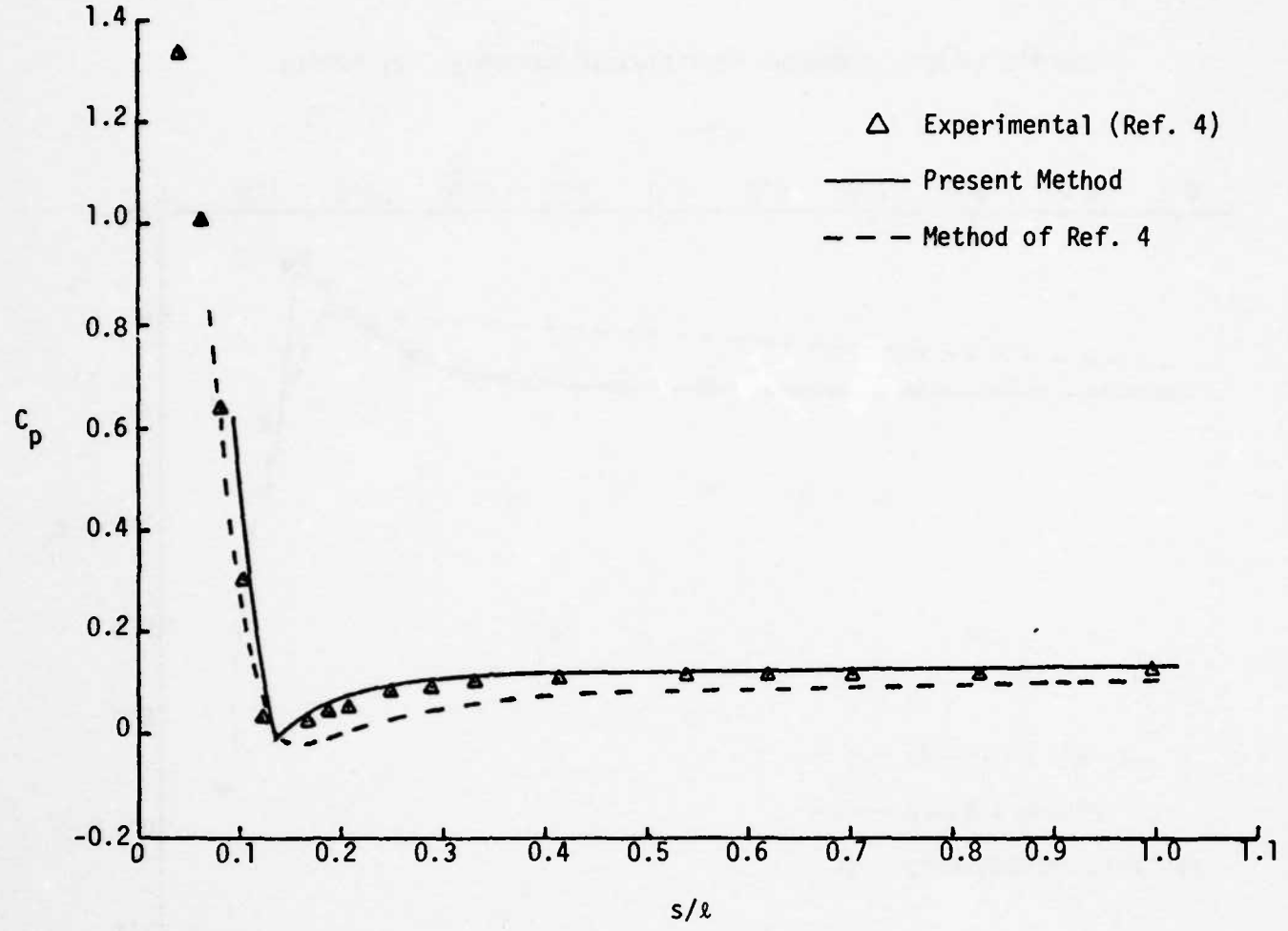

Figure 18. Pressure Distribution on Model 1, M_∞=1.9, α=0°

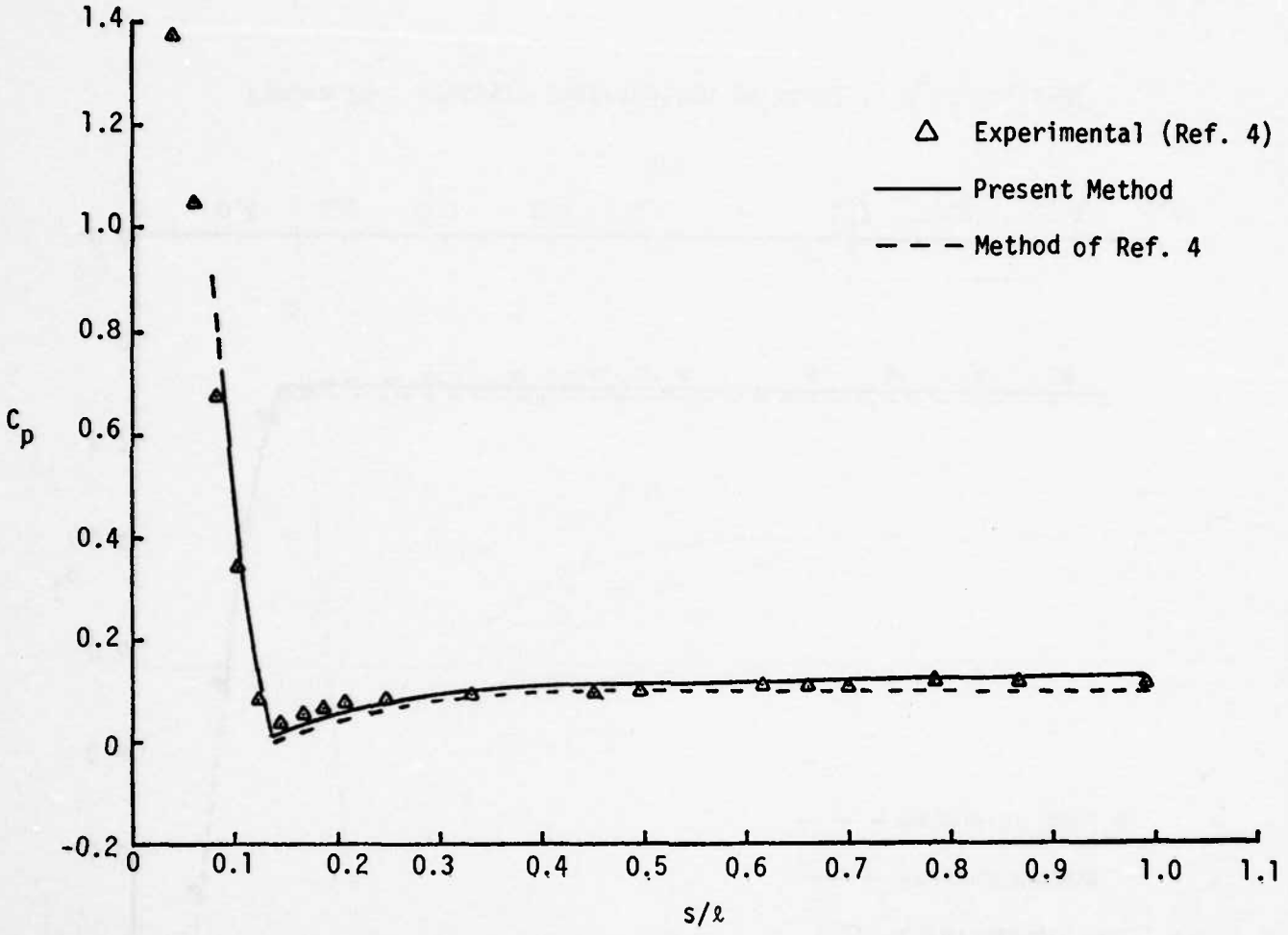

Figure 19. Pressure Distribution on Model 1, M_∞=2.3, α=0°

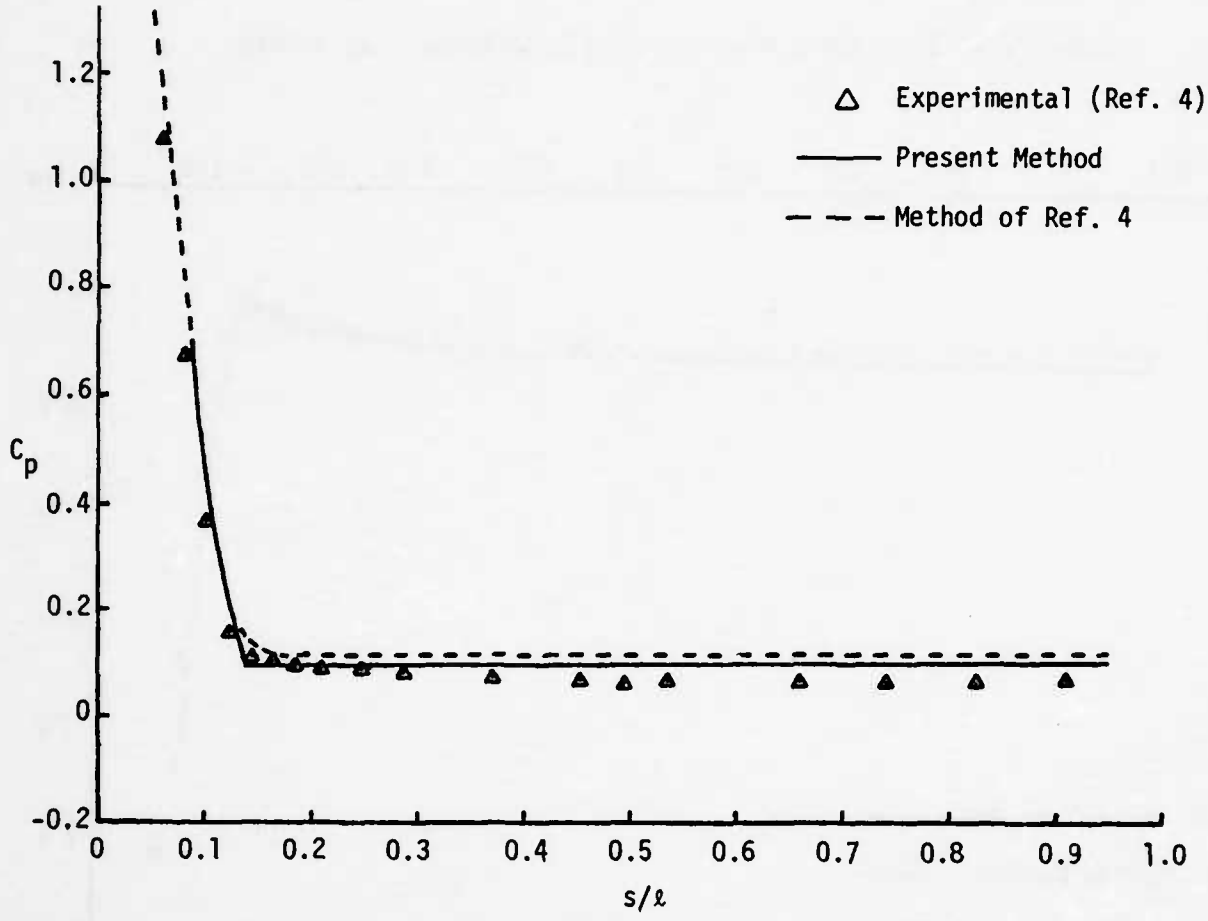

Figure 20. Pressure Distribution on Model 1, M_∞=4.63, α=0°

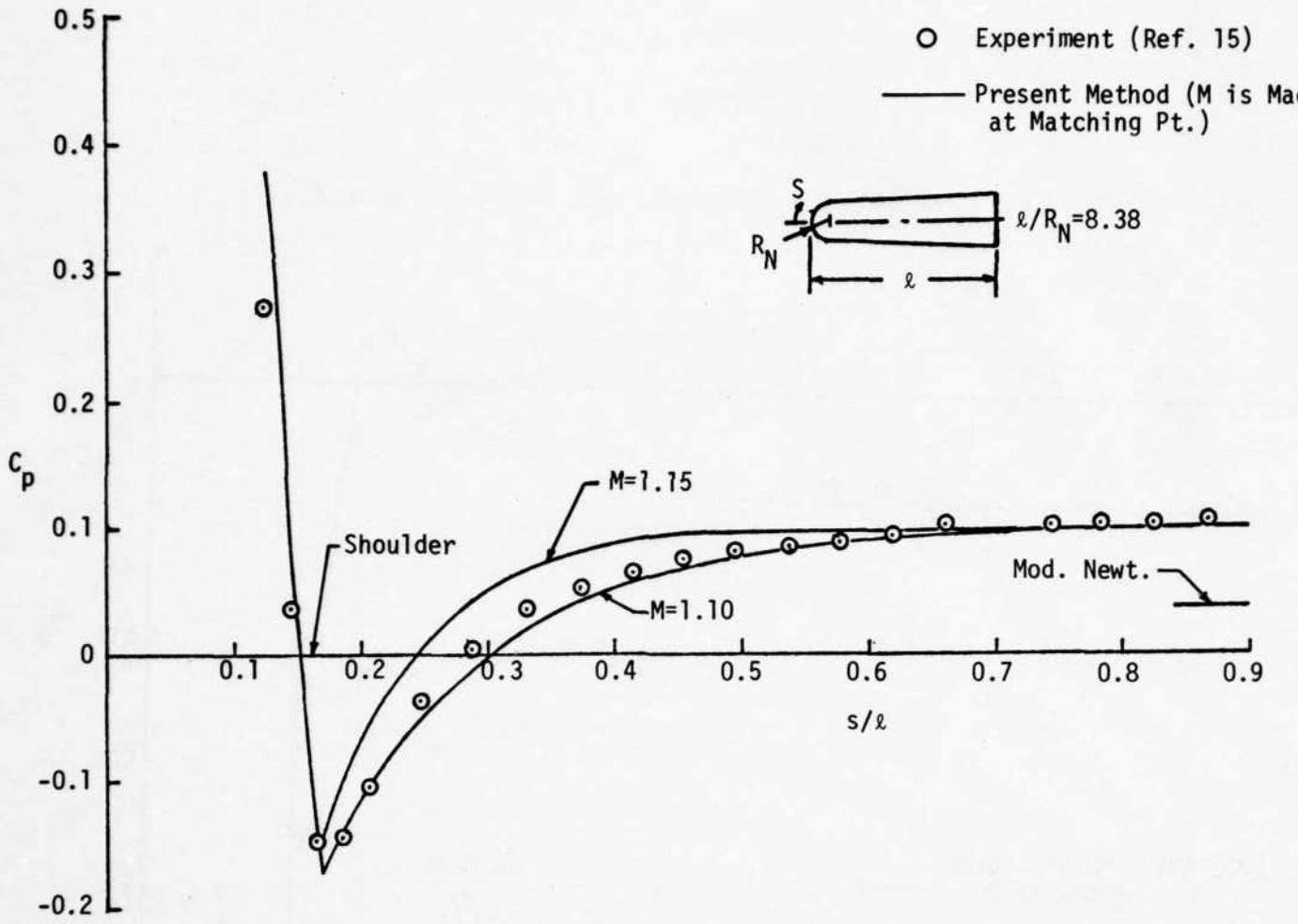

Figure 21. Pressure Distribution on Blunted Cone, δ_c=9°, M_∞=1.5, α=0°

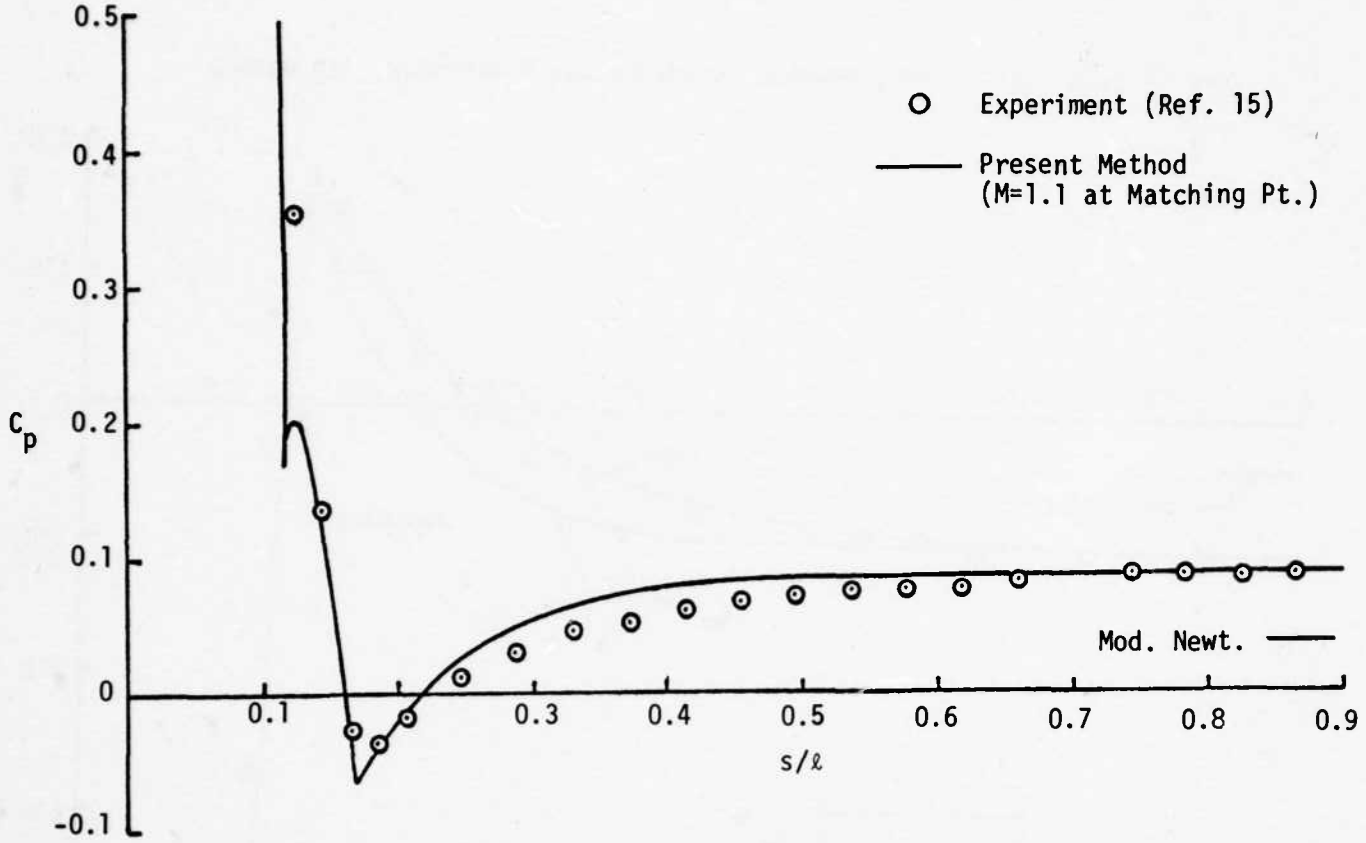

Figure 22. Pressure Distribution on Blunted Cone, δ_c=9°, M_∞=1.9, α=0

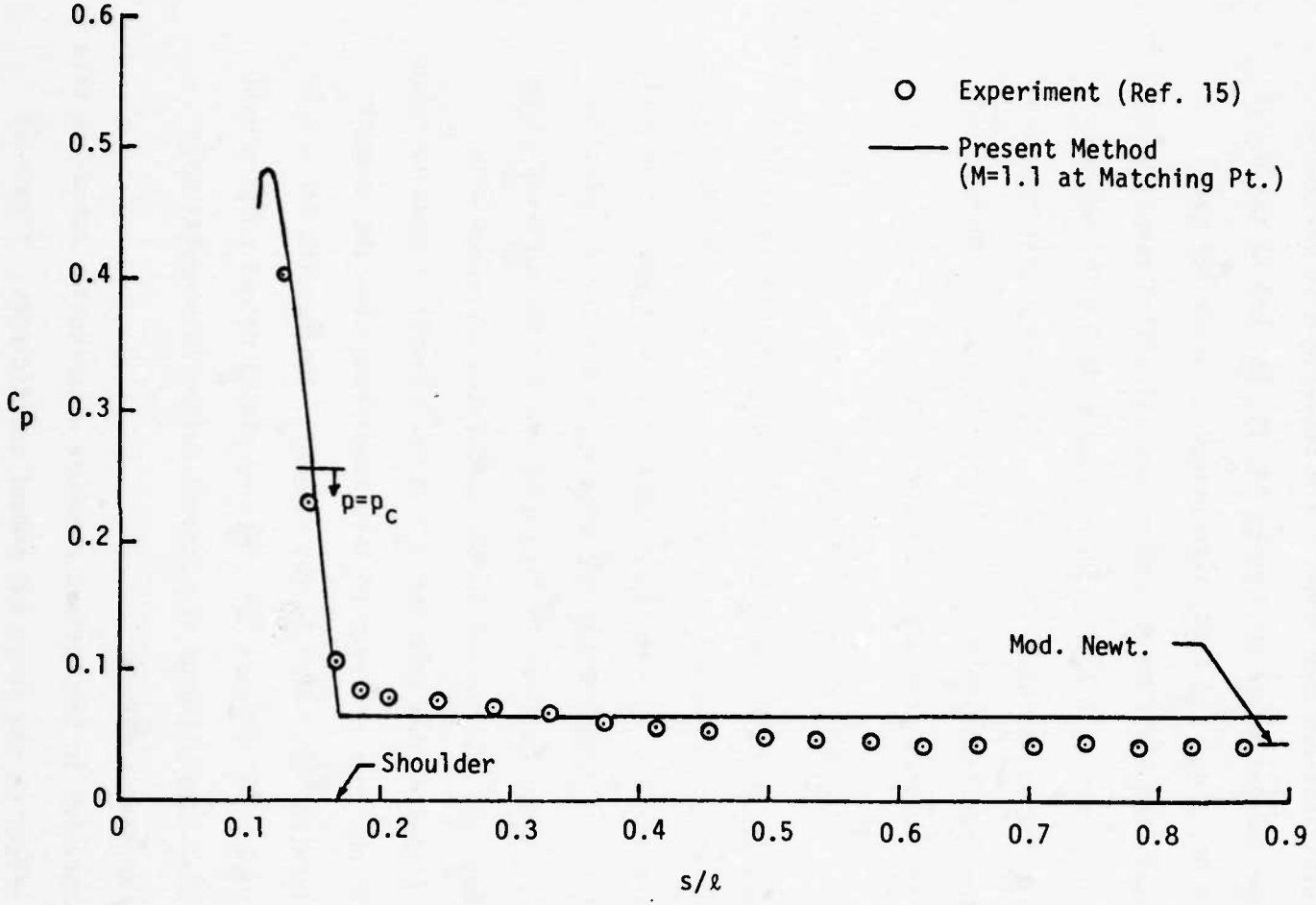

Figure 23. Pressure Distribution on Blunted Cone, $\delta_c=9°$, $M_\infty=4.63$, $\alpha=0$

Blunted Cone-Flare

Pressure distributions over Model 2 are compared with Jackson's theory[4] and experimental data[4] in Figures 24, 25, 26, and 27 for $\alpha = 0$ and $M_\infty = 2.3$, 2.96, 3.95, and 4.63, respectively. Since the over-expansion is small for these Mach numbers, the calculated results are close to Jackson's results. Both methods compare well with experimental data except near the beginning of the flare. It appears that boundary-layer separation occurs upstream of the flare and thus the theory does not calculate the correct pressure in this region.

Effect of Angle of Attack

Figures 28, 29, and 30 show the pressure distribution on the blunted 9° cone at $\alpha = 12°$ and $M_\infty = 1.5$ for $\theta = -90°$, 0°, and 90°. This example is a severe test for the theory because it is a small cone angle at an angle of attack greater than the cone angle and a low supersonic Mach number. The results given in Figure 28 are for the windward plane ($\theta = -90°$). Note the improvement in the calculated pressures when Equation (29) (labeled "new soln for p_c" in the figure) is used to calculate the equivalent cone pressure (p_c) in comparison with the tangent cone method (labeled "old soln" in the figure). The results for $\theta = 0°$ (Figure 29) and $\theta = 90°$ (Figure 30) (leeward plane) do not compare well with experimental data although the present method is somewhat more accurate than Jackson's method.

The inaccuracies in the surface pressure distribution appear to have only a small effect on the force and moment coefficients. Figure 31 gives the coefficients of pitching moment (C_M), normal (C_N), and axial force (C_A) as a function of angle of attack for Models 1 and 2. This

figure, the same results as Jackson's method, and the modified Newtonian theory predicts accurate results. However, this fact cannot, in general, be stated for other bodies over the Mach number range of interest.

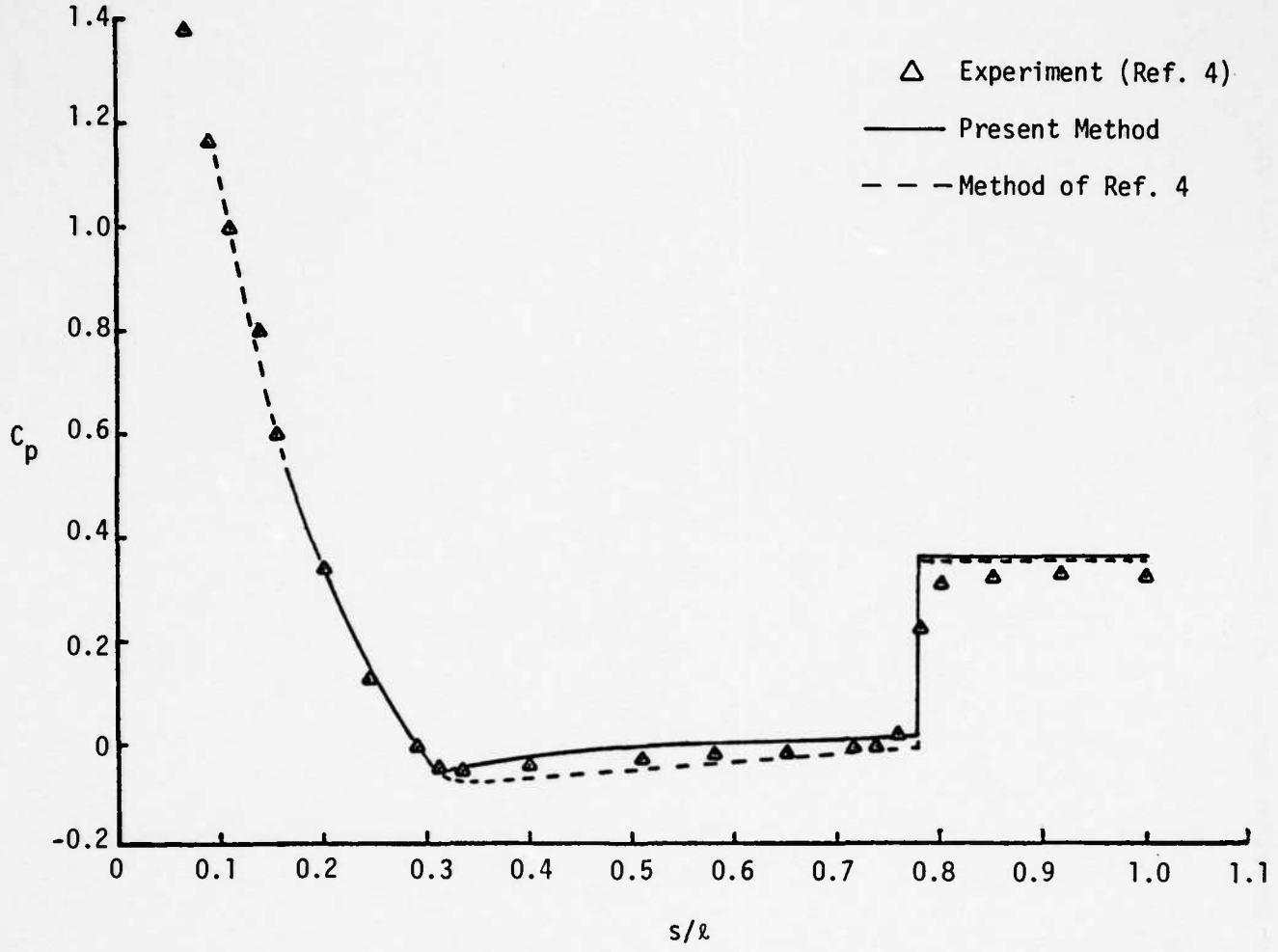

Figure 24. Pressure Distribution on Model 2, M_∞=2.3, α=0°

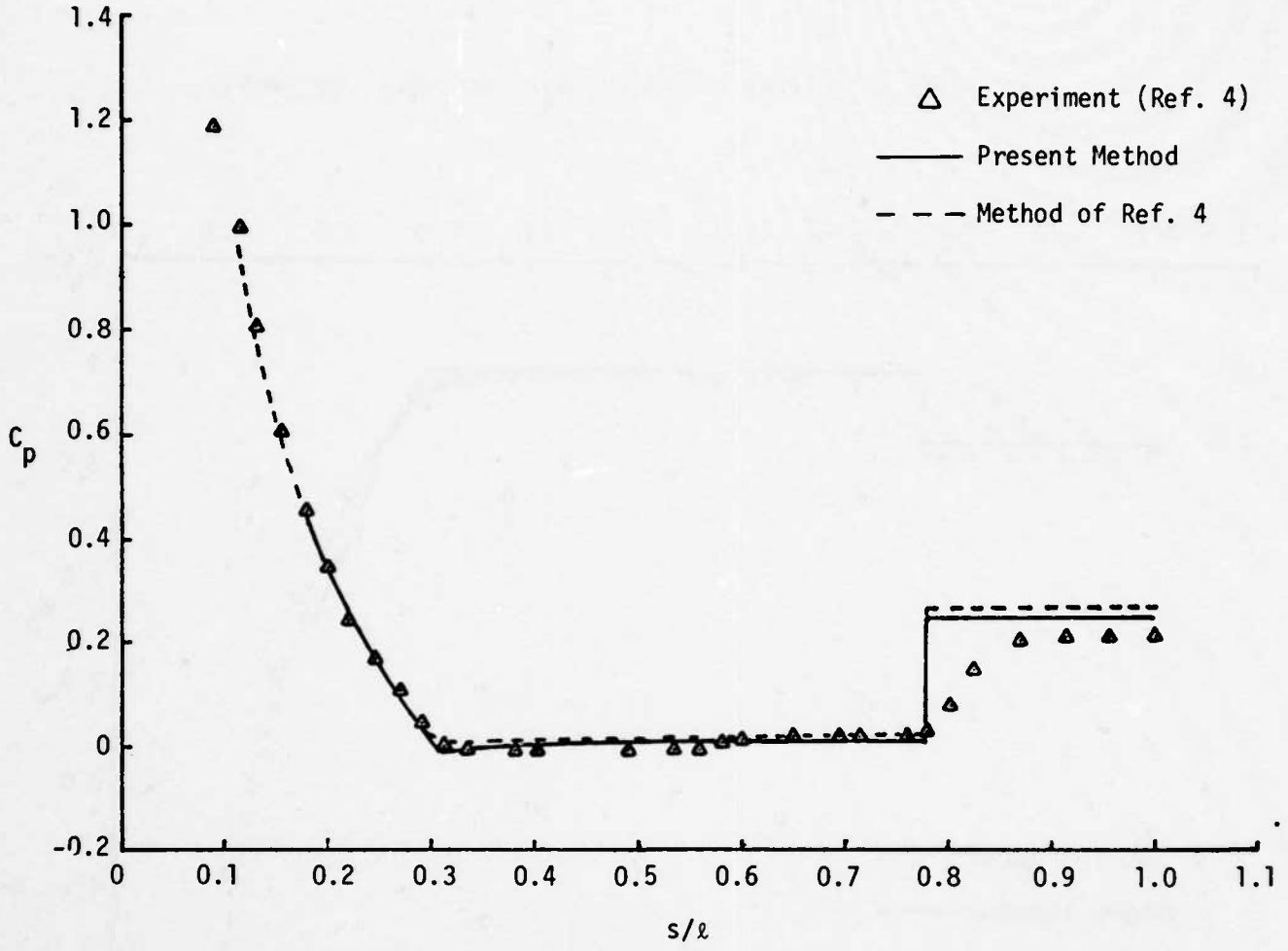

Figure 25. Pressure Distribution on Model 2, M_∞=2.96, α=0°

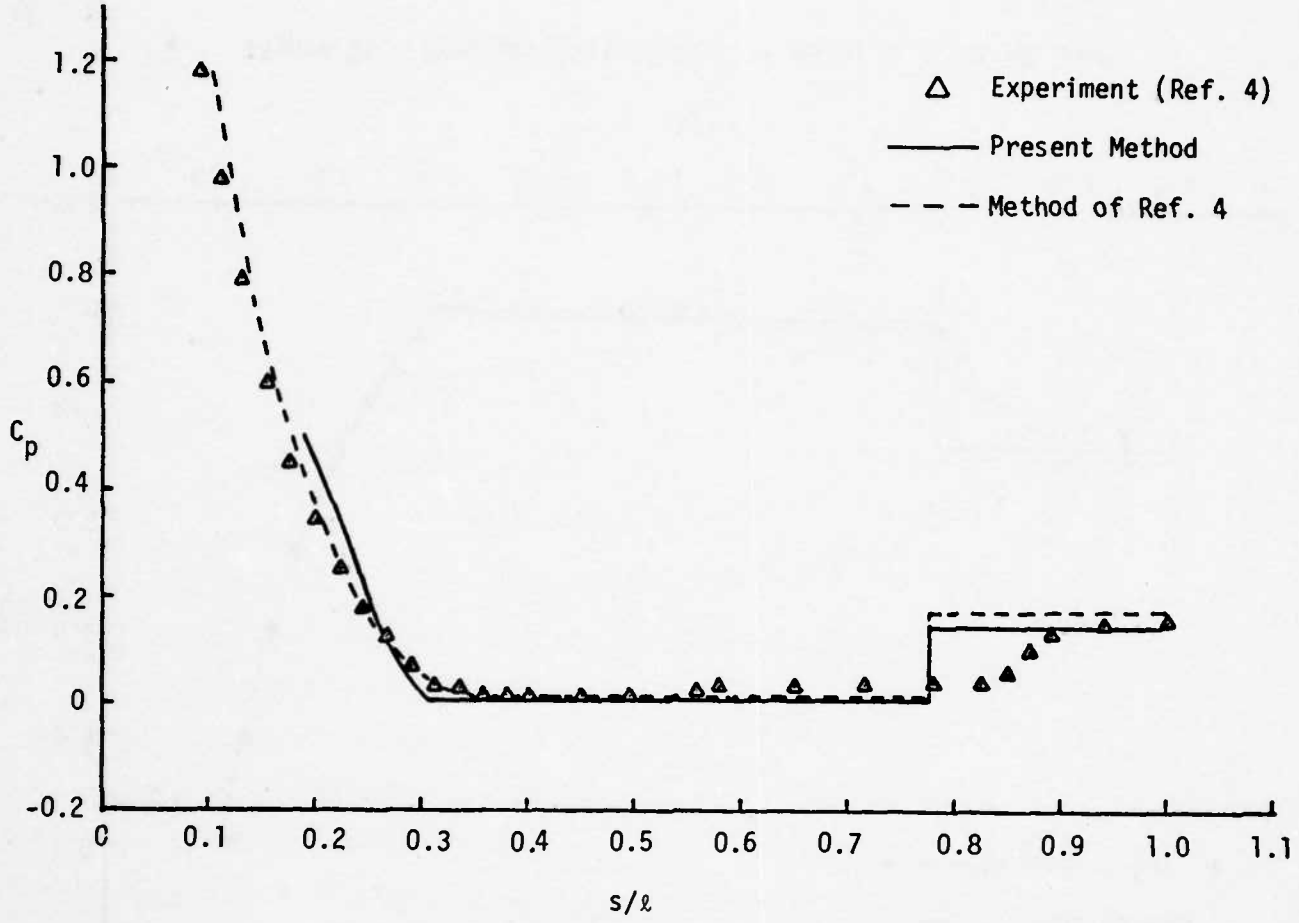

Figure 26. Pressure Distribution on Model 2, M_∞=3.95, α=0

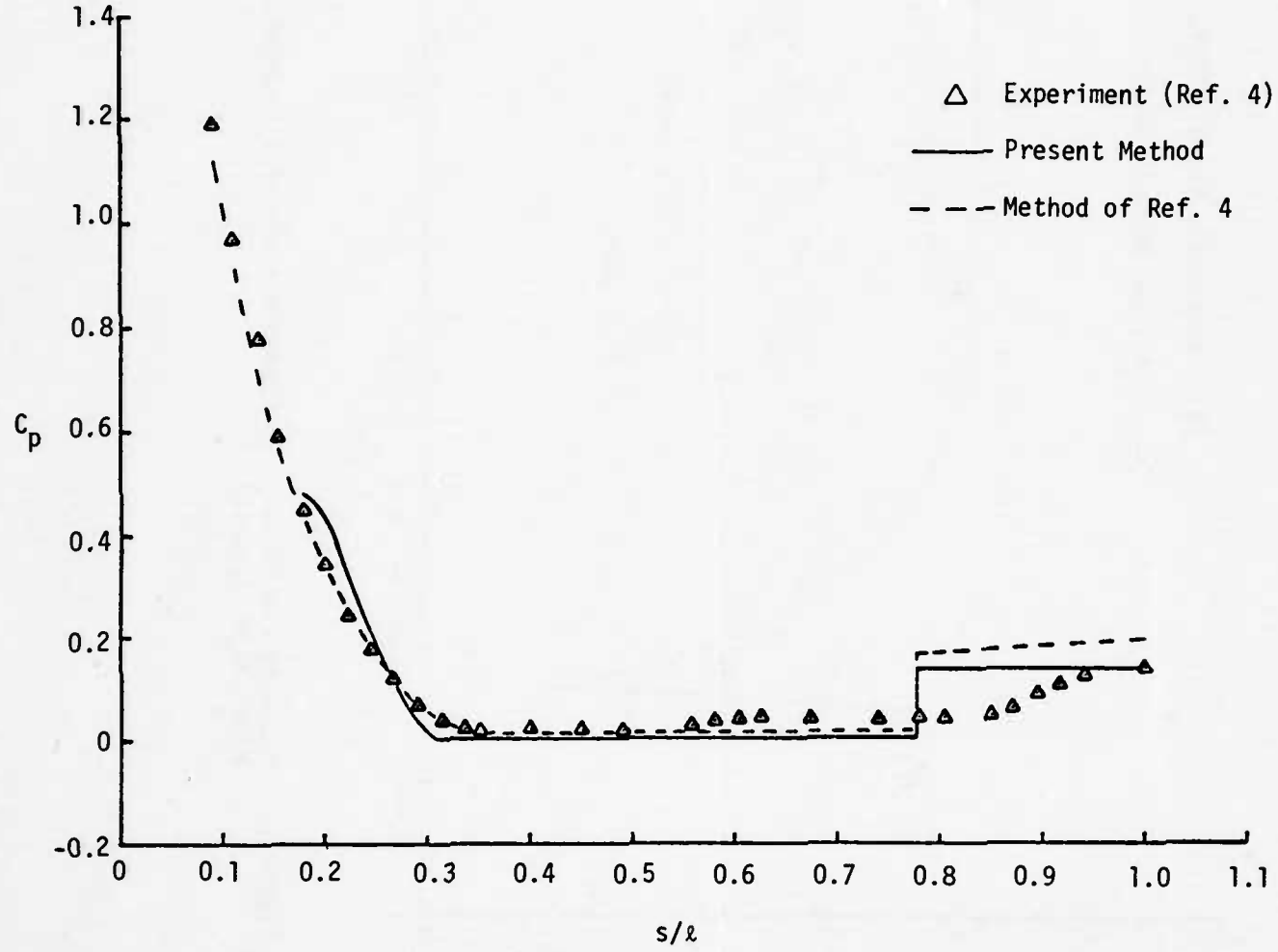

Figure 27. Pressure Distribution on Model 2, M_∞=4.63, α=0°

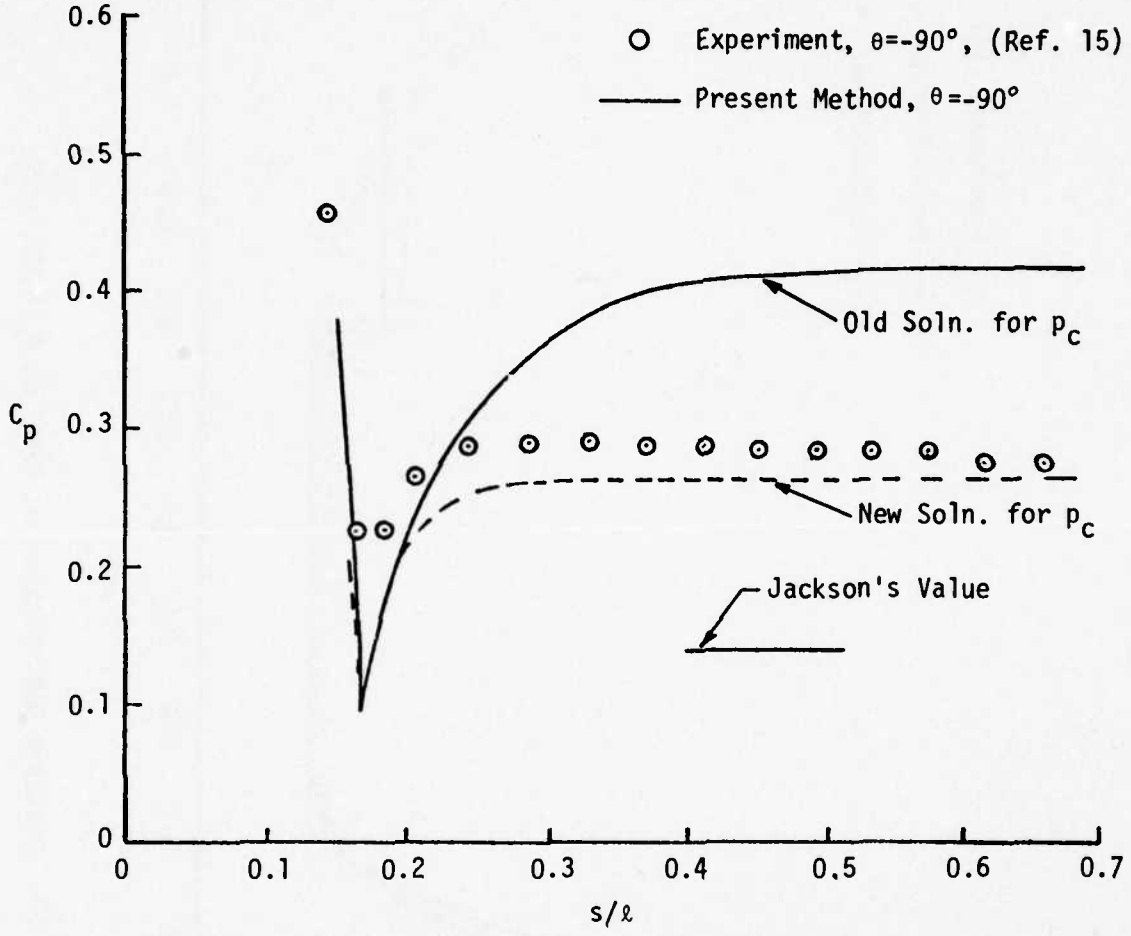

Figure 28. Pressure Distribution in Windward Plane of a Blunted Cone, δ_c=9°, M_∞=1.5, α=12°

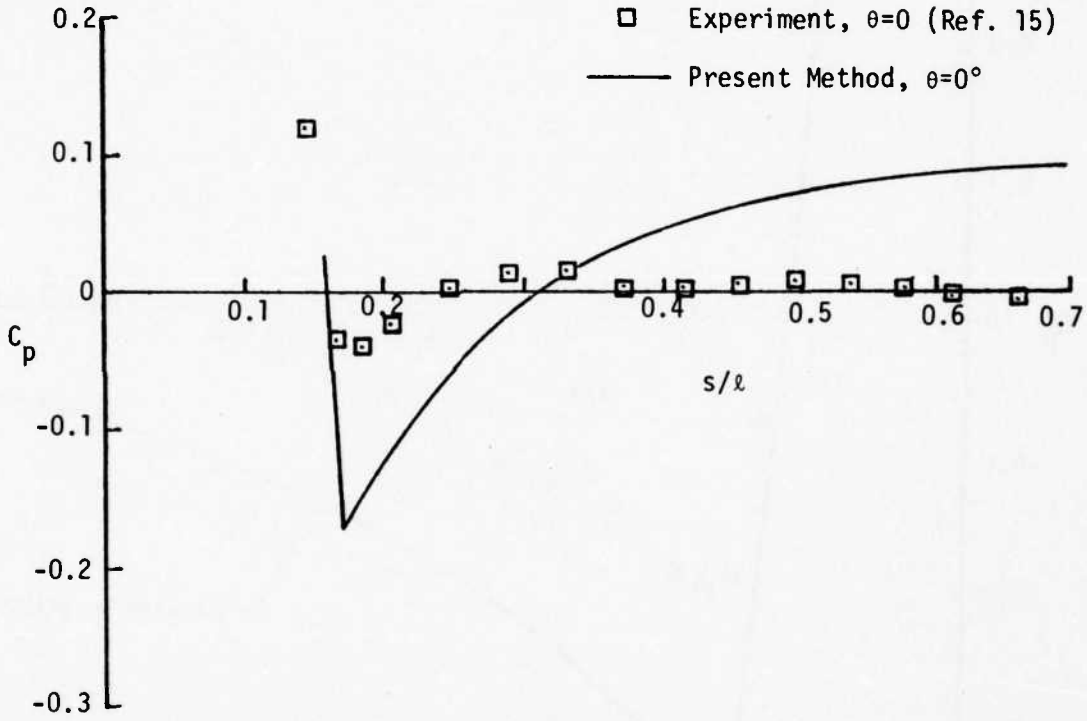

Figure 29. Pressure Distribution on Side Meridian of a Blunted Cone, δ_c=9°, M_∞=1.5, α=12°

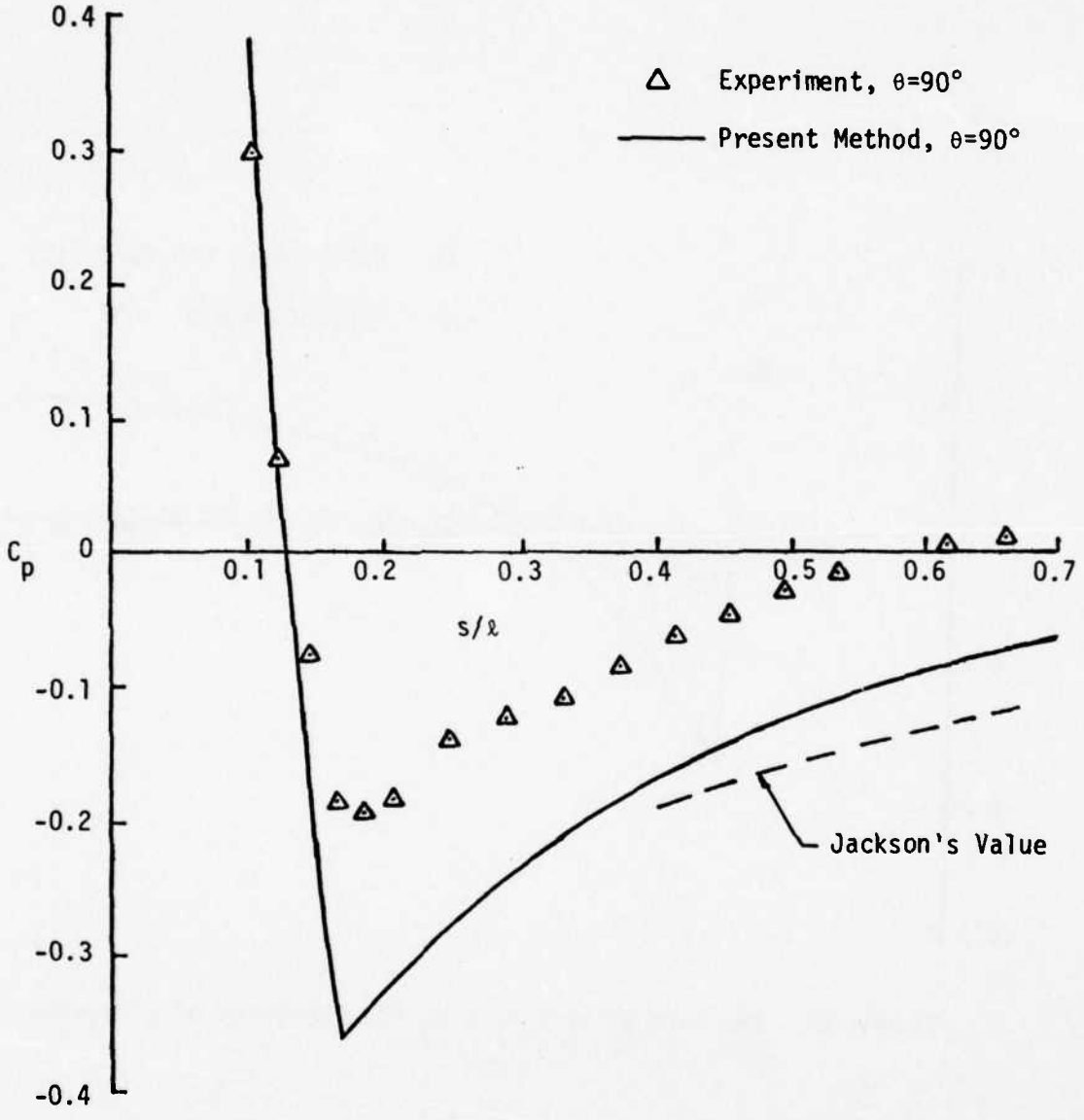

Figure 30. Pressure Distribution in Leeward Plane of a Blunted Cone, δ_c=9°, M_∞=1.5, α=12°

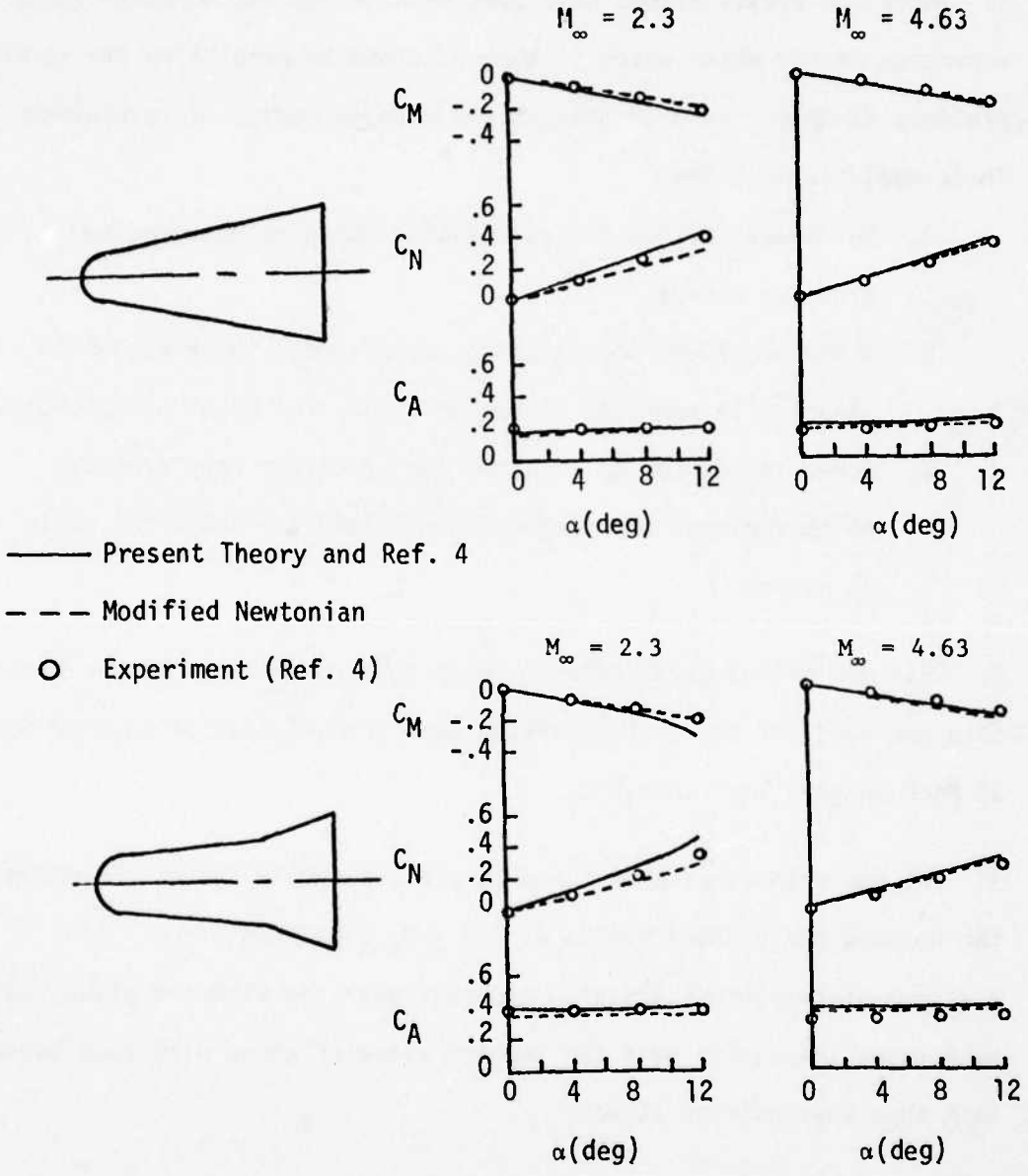

Figure 31. Comparison of Theory and Experiment for Models 1 and 2

CONCLUSIONS AND RECOMMENDATIONS

1. Three new modifications have been made to the second-order shock-expansion method which makes it more accurate in predicting the surface pressure distribution over pointed and blunted bodies of revolution. These modifications are:

   A. An "exact" method for calculating the pressure gradient around a corner.

   B. A new procedure for matching second-order shock-expansion theory with modified Newtonian theory for blunt nosed bodies.

   C. A new method for calculating the effective cone pressure which replaces the tangent-cone method for bodies at angle of attack.

2. This new method gives results which compare well with experimental data and predicts the over-expansion near the shoulder of blunted cones at Mach numbers less than 2.0.

3. The new method has been found to yield accurate forces and moments for pointed and blunted bodies at $1.5 \leq M_\infty \leq 4.63$ and $0 \leq \alpha \leq 12°$. Pressure distributions are also accurate near the windward plane, but tend to be inaccurate near the leeward plane of cones with cone angles less than the angle of attack.

4. It is recommended that additional results be calculated and compared with experimental data to determine the accuracy of the method at Mach numbers as low as 1.2. Also, modifications to the angle of attack solution are needed if accurate pressure near the leeward plane are desired.

REFERENCES

1. F. A. Woodward, "Analysis and Design of Wing-Body Combinations at Subsonic and Supersonic Speeds," Journal of Aircraft, Vol. 5, No. 6, 1968, pp. 528-534.

2. C. M. Jackson and R. S. Smith, "A Method for Determining the Total Drag of a Pointed Body of Revolution in Supersonic Flow with Turbulent Boundary Layer," NASA TN D-5046, 1969.

3. C. A. Syvertson and D. H. Dennis, "A Second-Order Shock-Expansion Method Applicable to Bodies of Revolution Near Zero Lift," NACA Report 1328, 1957.

4. C. M. Jackson, Jr., W. C. Sawyer, and R. S. Smith, "A Method for Determining Surface Pressure on Blunt Bodies of Revolution at Small Angles of Attack in Supersonic Flow," NASA TN D-4865, 1968.

5. B. F. Saffell, Jr., M. L. Howard, and E. N. Brooks, Jr., "A Method for Predicting the Static Aerodynamic Characteristics of Typical Missile Configurations for Angles-of-Attack to 180 Degrees," NSRDC Report 3645, 1971.

6. R. H. Whyte, "Spinner - A Computer Program for Predicting the Aerodynamic Coefficients of Spin Stabilized Projectiles," General Electric Class 2 Reports, 1969.

7. J. M. Solomon, M. Ciment, R. E. Ferguson, J. B. Bell, and A. B. Wardlaw, "A Program for Computing Steady Inviscid Three-Dimensional Supersonic Flow on Reentry Vehicles," - Vol. I: Analysis and Programming, NSWC/WOL/TR 77-28, Feb. 1977 and Vol. II: User's Manual, NSWC/WOL/TR 77-32, May 1977.

8. F. G. Moore and R. C. Swanson, Jr., "Aerodynamics of Tactical Weapons to Mach Number 3 and Angle of Attack 15°," Part I - Theory and Application, NSWC/DL TR-3584, Feb. 1977, and Part II - Computer Program and Usage, March 1977.

9. M. D. Van Dyke, "First and Second-Order Theory of Supersonic Flow Past Bodies of Revolution," JAS, Vol. 18, No. 3, March 1951, pp. 161-179.

10. S. H. Maslen, "Inviscid Hypersonic Flow Past Smooth Symmetric Bodies," AIAA Journal, Vol. 2, No. 6, 1964, pp. 1055-1061.

11. F. R. DeJarnette and H. H. Hamilton, "Aerodynamic Heating on 3-D Bodies Including the Effects of Entropy-Layer Swallowing," J. of Spacecraft and Rockets, Vol. 12, No. 1, 1975, pp. 5-12.

12. J. L. Sims, "Tables for Supersonic Flow Around Right Circular Cones at Zero Angle of Attack," NASA SP-3004, 1964.

13. N. H. Johannsen and R. E. Meyer, "Axially-Symmetrical Supersonic Flow Near the Center of an Expansion," Aero. Quart., Vol. II, August 1950, pp. 127-142.

14. A. M. Morrison, J. M. Solomon, M. Ciment, and R. E. Ferguson, "Handbook of Inviscid Sphere-Cone Flow Fields and Pressure Distributions, Volumes I and II," NSWC/WOL/TR 75-45, December 1975.

15. W. C. Sawyer and R. S. Smith, "Experimental Surface-Pressure Distributions on a 9° Spherically Blunted Cone at Mach Numbers from 1.50 to 4.63," NASA TM X-1730, 1968.

APPENDIX A

Evaluation of Distance Along a Streamline at a Corner

In order to determine the "exact" pressure gradient downstream of a corner, the differential of length along a streamline is needed. Referring to Figure A1,

$$ds_A = \frac{a\, d\beta}{\sin \mu} \tag{A1}$$

$$d\beta = -d\delta_o - d\mu = d\nu - d\mu$$

Thus, Equation (A1) becomes

$$\frac{ds_A}{d\delta_o} = \frac{a}{\sin \mu}\left(\frac{d\mu}{d\nu} - 1\right) \tag{A2}$$

But from the definition of μ and ν it follows that

$$\frac{d\mu}{d\nu} = +1 - \frac{\left(\frac{\gamma+1}{2}\right) M^2}{(M^2-1)} \tag{A3}$$

Use this result in Equation (A2) to get

$$\frac{ds_A}{d\delta_o} = -a\,\frac{\left(\frac{\gamma+1}{2}\right) M^3}{(M^2-1)} \tag{A4}$$

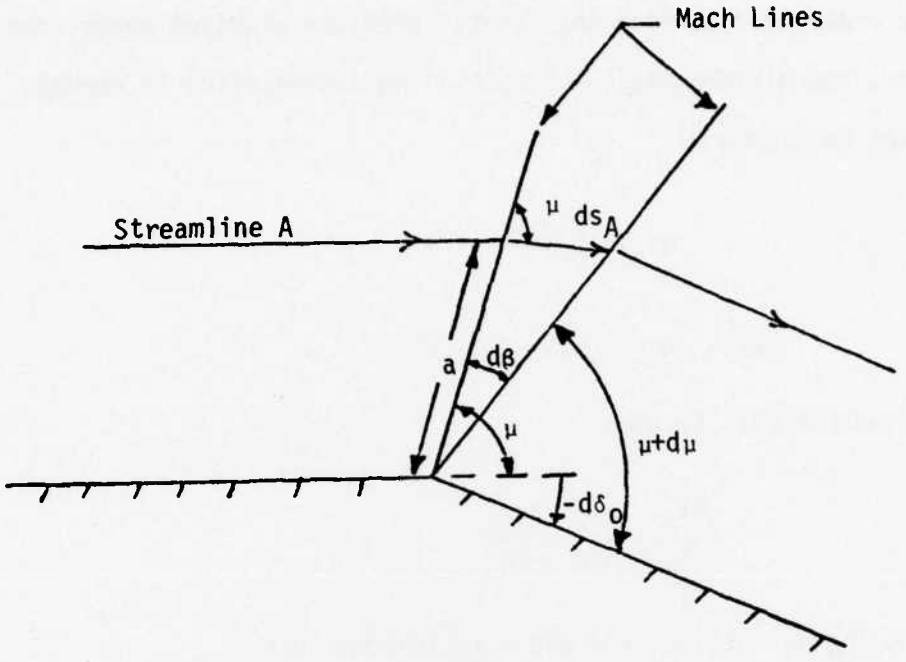

Figure A1. Arc Length Around a Corner

GLOSSARY OF TERMS

a	distance from body to streamline A
B	function defined by Equation (4)
C_A	axial-force coefficient
C_M	pitching-moment coefficient
C_N	normal-force coefficient
C_p	pressure coefficient, $C_p = 2(p-p_\infty)/(\rho_\infty V_\infty^2)$
C_1, C_2	characteristic coordinate
ℓ	body length (calibers)
M	Mach number
n	coordinate normal to a streamline (calibers)
p	static pressure ($dyne/cm^2$)
p_t	total pressure at stagnation point($dyne/cm^2$)
Q	function defined by Equation (17)
r	radius of body of revolution (calibers)
R	body radius of curvature (calibers)
s	coordinate along a streamline (calibers)
x	coordinate along body axis (calibers)
y	coordinate normal to x in plane of symmetry, see Figure 10 (calibers)
α	angle of attack (degrees)
γ	ratio of specific heats (1.4 for air)
δ	flow inclination angle and cone angle (degrees)
η	function defined by Equation (2)
θ	meridian angle, see Figure 10 (degrees)
λ	function defined by Equation (5)
μ	Mach angle, $\mu = \sin^{-1}(1/M)$
ν	Prandtl-Meyer expansion angle (degrees)

ϕ	angle on sphere measured from nose (degrees), see Figure 7
Ω	ratio of cross-sectional area of streamtube to that at M=1, see Equation (6)

Subscripts

1	condition at start of Prandtl-Meyer Expansion
2	condition at end of Prandtl-Meyer Expansion
o	surface streamline
o_1	beginning of the expansion on the surface
A	streamline off the surface
c	quantities evaluated for cone tangent to the body
eq	refers to equivalent cone quantities
MN	modified Newtonian value
N	nose
w	refers to wind axes
∞	free stream conditions

Superscripts

*	evaluated where M=1

DISTRIBUTION

Commander
Naval Sea Systems Command
Washington, DC 20360
ATTN: SEA-03 (Mr. Lionel Pasiuk)
Library (2)

Commander
Naval Air Systems Command
Washington, DC 20361
ATTN: AIR-320 (Mr. Bill Volz)
AIR-320 (Dr. H. Mueller)
AIR-532
Library (2)

Chief of Naval Research
Arlington, VA 22217
ATTN: Mr. Lawrence E. McCullough
Mr. Dave Seigel
Dr. Bob Whitehead
Dr. R. J. Lundegard
Mr. Mort Cooper
Mr. Ralph Cooper
Library (2)

Chief of Naval Operations
Pentagon
Washington, DC 20350
ATTN: OP-098
Library (2)

Commander
Naval Material Command
Washington, DC 20360
ATTN: MAT-032 (Mr. Sid Jacobson)
Dr. John Huth
Library (2)

Commander
Naval Weapons Center
China Lake, CA 93555
ATTN: Mr. Ray Van Aken
Mr. D. Meeker
Mr. Kinge-Okauchi
Library (2)

Commander
Pacific Missile Test Center
Point Mugu, CA 93041
ATTN: Mr. Joe Rom
Library (2)

Commander
David W. Taylor Naval Ship Research
and Development Center
Bethesda, MD 20084
ATTN: Dr. T. C. Tai
Library (2)

Commander
Naval Air Development Center
Warminster, PA 18974
ATTN: Mr. Bill Langen
Library (2)

Commanding Officer
Naval Ordnance Station
Indian Head, MD 20640

Commandant of the Marine Corps
Headquarters, Marine Corps
Washington, DC 20380

Commander
Naval Air Engineering Center
Aeronautical Structures Department
Lakehurst, NJ 19112

Commander
Naval Air Test Center
Patuxent River, MD 20670
ATTN: Mr. Ron Wilson
Library (2)

Commander
Naval Coastal Systems Laboratory
Panama City, FL 32401 (2)

Commander
Naval Ocean Systems Center
San Diego, CA 92135 (2)

Commander
Naval Underwater Systems Center
Newport, RI 02480 (2)

Headquarters
Air Force Systems Command
Andrews Air Force Base, MD 20331

Headquarters, USAF
Washington, DC 20330

U. S. Air Force Systems Command
Regional Offices
c/o Department of the Navy
Washington, DC 20360

Air Force Armament Laboratory
Eglin Air Force Base, FL 32542
ATTN: Dr. D. Daniel
Dr. S. G. Pallas
Mr. C. Butler
Dr. Lijewski
Mr. C. Mathews
Mr. K. Cobb
Mr. E. Sears
Library (2)

USAF Academy
Colorado Springs, CO 80912 (2)

Air Development and Test Center
Eglin Air Force Base, FL 32542 (2)

Arnold Engineering Development Center
USAF
Tullahoma, TN 37389
ATTN: Mr. J. Usselton
Mr. W. B. Baker, Jr.
Library (2)

Edwards Air Force Base
Edwards, CA 93523
ATTN: Flight Research Center
Rocket Propulsion Laboratory
(Maj. Washburn)
Library (2)

Wright Patterson Air Force Base
Dayton, OH 45433
ATTN: Aeronautical Systems Division (2)
Aeronautical Research Laboratory
Air Force Flight Dynamics
Laboratory
FGC (Mr. E. Flinn)
(Dr. G. Kurylowich)
(Dr. V. Hoehne)
FX (Mr. Mel Buck)
Library (2)

ARO Inc.
Arnold Air Force Station, TN 37389
ATTN: Dr. Tsuying Hsieh

Sandia Laboratories
Albuquerque, NM 87115
ATTN: Division 1331 (Mr. Robert LaFarge)
Library

Sandia Laboratories
Box 969
Livermore, CA 94550
ATTN: Division 8158
Library

The Rand Corporation
1600 Main Street
Santa Monica, CA 90406

Stanford Research Institute
Menlo Park, CA 94025
ATTN: Dr. Milton Van Dyke
Library (2)

Raytheon Company
Spencer Laboratory
Burlington, MA 01803
ATTN: BOX SL 7162 (Mr. Steve Pearlsing)

McDonnell Douglas Astronautics Co. (West)
5301 Bolsa Avenue
Hunington Beach, CA 92647
ATTN: Mail Station 13-2 (Dr. Jim Zerikos)

Vought Corporation
P. O. Box 5907
Dallas, TX 75222
ATTN: Dr. W. B. Brooks
Mr. F. Prilliman

Boeing Computer Services, Inc.
P. O. Box 24346, M/S 8F-37
Seattle, WA 98124
ATTN: Mr. Roger Wyrick

Lockheed Missiles and Space Co., Inc.
P. O. Box 1103, W. Street
Huntsville, AL 35807
ATTN: Mr. B. H. Shirley

Lockheed Missiles and Space Co., Inc.
Department 81-10, Bldg. 154
Sunnyvale, CA 94088
ATTN: Dr. Lars E. Ericson
Mr. P. Reding

Nielsen Engineering and Research, Inc.
510 Clyde Avenue
Mountain View, CA 94043
ATTN: Dr. Jack Nielsen

Mr. V. L. Pianta
P. O. Box 1201
San Jose, CA 95108

Virginia Polytechnic Institute and
State University
Department of Aerospace Engineering
Blacksburg, VA 24060
ATTN: Prof. J. A. Schetz
Prof. A. H. Nayfeh
Library (2)

North Carolina State University
Department of Mechanical and
Aerospace Engineering
Box 5246
Raleigh, NC 27607
ATTN: Prof. F. R. DeJarnette (10)
Library (2)

University of Tennessee Space Institute
Tullahoma, TN 37388
ATTN: Dr. J. M. Wu
Library (2)

Defense Documentation Center
Cameron Station
Alexandria, VA 22314 (12)

Library of Congress
Washington, DC 20390
ATTN: Gift and Exchange Division (4)

Defense Printing Service
Washington Navy Yard
Washington, DC 20374

Advanced Research Projects Agency
Department of Defense
Washington, DC 20305 (2)

Director
Defense Research and Engineering
Department of Defense
Washington, DC 20305
ATTN: R&AT Office (Mr. B. Osborne)
Library (2)

Headquarters, NASA
Washington, DC 20546

NASA George C. Marshal Flight Center
Huntsville, AL 35804

NASA Goddard Space Center
Greenbelt, MD 20771

NASA Lewis Research Center
Cleveland, OH 44101

NASA Ames Research Center
Moffett Field, CA 94035
ATTN: Mr. Vic Peterson
Mr. John Rakich
Library (2)

NASA Langley Research Center
Langley Station
Hampton, VA 23365
ATTN: Dr. Roy C. Swanson, Jr.
Mr. Bud Bobbitt
Mr. Jerry South
Mr. Leroy Spearman
Mr. C. M. Jackson, Jr.
Mr. W. C. Sawyer
Library (2)

Applied Physics Laboratory
Johns-Hopkins University
8621 Georgia Avenue
Silver Spring, MD 20910
ATTN: Dr. L. L. Cronvich
Mr. Edward T. Marley
Dr. Gordon Dugger
Library (2)

Director, U. S. Army
Ballistic Research Laboratory
Aberdeen Proving Ground, MD 21005
ATTN: Dr. C. H. Murphy
Mr. L. McAllister
Mr. A. Platou
Mr. B. McCoy
Library (2)

President
U. S. Army Field Artillery Board
Fort Sill, OK 73503
ATTN: Marine Corps Liaison Officer
Library (2)

Commander
U. S. Army Material Development and
Readiness Command
5001 Eisenhower Avenue
Alexandria, VA 22333

Commander
Frankford Arsenal
Philadelphia, PA 19137
ATTN: Mr. W. Gadomski
Library (2)

Commander
Harry Diamond Laboratories
2800 Powder Mill Road
Adelphi, MD 20783
ATTN: Technical Library (2)

Commander
U. S. Army Combat Development Command
Field Artillery Agency
Fort Sill, OK 73503 (2)

Commander
U. S. Army Missile Command
Redstone Aresenal, AL 35809
ATTN: DRSMI (Mr. Ray Deep)
DRSMI (Dr. D. J. Spring)
Library (2)

AF Office of Scientific Research
Washington, DC 20330
ATTN: Library (2)

Naval Research Laboratory
Washington, DC 20375 (2)

Superintendent
U. S. Naval Academy
Annapolis, MD 21402
ATTN: Head, Weapons Department
Head, Science Department
Library (2)

Superintendent
U. S. Naval Postgraduate School
Monterey, CA 95076
ATTN: Head, Mechanical Engineering
Department
Head, Department of Aeronautics
Library (2)

Chief of Naval Research
Department of the Navy
Washington, DC 20360

Director
Naval Strategic Systems Projects
Office (PM-1)
Department of the Navy
Washington, DC 20360 (2)

Officer in Charge
U. S. Naval Scientific and
Technical Intelligence Center
U. S. Naval Observatory
Washington, DC 20360 (2)

Commander
Marine Corps Development and
Education Command
Quantico, VA 22134
ATTN: Director, Development Center
S&R Division
Air Operations Division
Ground Operations Division
Library (2)

U. S. Army Armament Research and
Development Command
Dover, NJ 07801
ATTN: Mr. E. F. Friedman
Mr. Henry Hudgins
Mr. M. Cline
Mr. A. Loeb
Mr. Mertz
Library

LOCAL

E41
G
G20
G23
G30
G40
G41 (Mr. B. Piper, Mr. G. Graff)
K
K02
K04
K05
K20
K21 (Dr. J. Sun, Dr. F. G. Moore) (20)
K22
K23 (Mr. J. Mitchell)
K50
K80 (Mr. S. Hastings)
K81 (Dr. M. Krumins) (2)
K81 (Mr. F. Baltakis)
K82 (Dr. J. Goeller, Dr. N. Sheets,
Mr. F. Regan)
R
R44 (Dr. J. Solomon)
X210 (2)


ATE
LMED
7